國立交通大學

電信工程研究所

碩士論文

車用前視防撞雷達之可切換波束天線陣列

77GHz Beam-Switching Antenna Array for
Forward-Looking Collision Avoidance System

研究生：鄭怡力

指導教授：鍾世忠　博士

中華民國九十三年六月

車用前視防撞雷達之可切換波束天線陣列

研究生：鄭怡力　　　　　　　指導教授：鍾世忠 博士

國立交通大學電信工程研究所

摘要

　　本論文進行有關 77GHz FMCW (Frequency Modulation Continuous Wave) 車載前視防撞雷達系統中天線陣列的設計。發展一平面印刷式微帶天線 (microstrip antenna)陣列。此天線陣列由印刷電路形式之 Rotman Lens 饋入，利用不同輸入點在陣列輸入面上造成對應的相位差以提供數個可供選擇切換的主輻射波束方向。此天線陣列係由數個雙排天線次陣列組成，饋入功率經由一功率分配器平均分配至下層兩排子陣列。每一排子陣列由數十個串聯饋入(series fed)之微帶天線組成串接微帶天線次陣列，設計時在寬度上漸次變化以限制其旁波大小，使其在電場平面方向波束寬約 5 度，旁波較主波小 15dB，在磁場平面方向可由 Rotman Lens 之不同輸入點在 0 度與正負 7.5 度選擇不同的主輻射波束。

77GHz Beam-Switching Antenna Array for

Forward-Looking Collision Avoidance System

Student: Yi-Li Cheng   Advisor: Dr. Shyh-Jong Chung

Institute of Communication Engineering

National Chiao Tung University

Abstract

A planner printed antenna array for 77GHz FMCW mobile forward-looking collision avoidance system is presented in this thesis. This antenna array is fed with a printed Rotman lens which provides different output beam directions respect to different input ports. The antenna array includes several antenna sub-arrays; each sub-array comprises a power divider and two antenna rows. The antenna row contains tens of series fed tapered microstrip antennas, to keep the main beam of E-plane within 5°and the side lobe level bellow then 15dB. Due to Rotman Lens, the direction of main beam of the integral antenna array can be switched between 0°,7.5°,-7.5°.

Acknowledgement

　　兩年在交大電信所的日子，不但讓我學到了微波工程的專業知識，更重要的是學到了求學的態度與方法。特別是我的指導教授─鍾世忠博士不論是在專業學養或是處事態度上都讓我獲益良多。

　　在 912 實驗室有如置身於一個大家庭，感謝實驗室的學長怡陽、卓如、敏銓、彥瑋、杰霖、耀賢、俊仰、南君、智軒；同學小雅、丹雄、阿全、明洲、伸憶、俊甫、揚裕、凱得與學弟妹侑信、民仲、清文在學業與生活上都給了我很多建議也一起分享了這兩年來快樂的時光。

　　最後，我要感謝家人、驥瑋、珮如的支持，因為你們毫無保留的支持與鼓勵，讓我能安安穩穩的完成這篇論文。

Content

List of Figures

List of Tables

Chapter 1. Introduction

Advanced vehicle control and safety system is getting more important because of the increasing traffic. Collision avoidance Radar is the key component of the system, the radar for vehicle applications provides drivers the information of the other vehicles, pedestrian, and other hazardous objects. The overall vehicle collision avoidance radar system generally contains forward-looking radar, sideward-looking radar, and backward-looking radar. The mission of backward-looking radar and sideward-looking radar is to prevent crash and collision when changing lanes by detecting two sides and backward objects. Both sideward-looking radar and backward-looking radar detect only for target existence, but forward-looking radar needs to collect information about velocity, distance, and angular position of targets in front of the system, it leads the techniques required for forward-looking radar is much high then sideward-looking radar and backward-looking radar.

1.1 Requirements of Forward-looking Radars
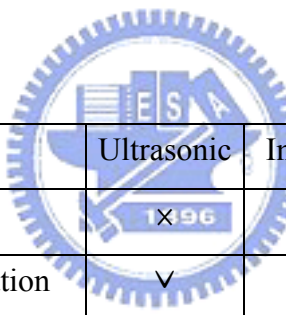
Several sensing technique, e.g. ultrasonic, lasers, IR (infrared rays), cameras, microwaves, and millimeter-waves can be chosen for forward-looking radars, but there are some requirements for forward-looking radars valid for practical application situations: [1]

- Sufficient maximum range and high sensitivity
- Simultaneous measurement of object range and relative radial velocity

- Multi-target sensing capability

- High measuring update rate

- Large azimuth range with good discrimination

- Small sensor dimensions and mounting without impact on styling

- Immunity against bad weather and dirt contamination

- Low cost at large production volumes

To satisfy these requirements, millimeter-wave technique is the most appropriate solution for forward-looking radar applications; the contrast table of these different techniques is shown in table 1.1. Millimeter-wave technique operates with high immunity with raindrop, fog, dust, etc., on the other hand, millimeter-wave technique forms main beam within 5° with acceptable size due to its high operating frequency and short wavelength.

	Ultrasonic	Infra-red	Video	Radar
Range	×	∨ ∨	∨ ∨	∨ ∨
Range Accuracy and Resolution	∨	∨	∨	∨ ∨
Angular Accuracy and Resolution	Multi-sensor	Multi-beam	∨ ∨	∨
Static/Dynamic Detection	∨	∨ ∨	∨ ∨	∨
Object Range Rate/Velocity	××	∨ ∨	∨	∨ ∨
Object Size/Extent Estimate	××	∨ ∨	∨ ∨	∨
Obscuration	∨	××	××	∨ ∨
Size/Packaging	×	∨	∨	∨
Cost	∨	∨	∨	×
Technology maturity	∨	∨	∨	∨

Table 1.1: contrast between several sensing technique

1.2 About this Thesis

Accurate beam scanning ability is a significant property of radar system. For forward-looking radar system in our scheme, the antenna provide 3~5 main beams to detect target in front and the adjacent lanes, this implies that the beam scans in a range of $\pm 7^{\circ}$, as shown in figure 1-1.
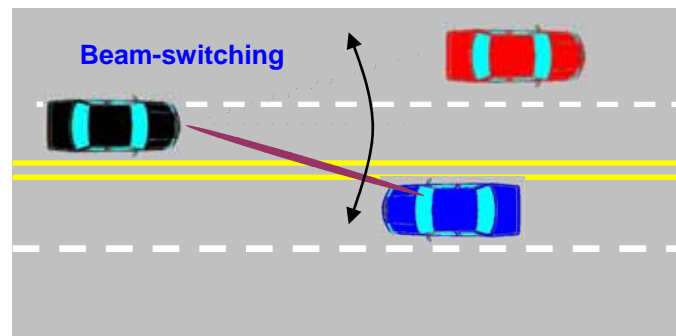
Fig. 1-1: beam-switching antenna

The purpose of this thesis is to develop a switch-able narrow beam antenna for forward-look radar application. The antenna comprises a microstrip antenna array and a Rotman lens in the character of beam former. Chapter 2 presents the theory of antenna array and design; chapter 3 describes the theory and design of microstrip antenna; chapter 4 shows the development and design of Rotman Lens; and conclusions are followed in chapter 5.

Chapter 2　Antenna Array

To achieve narrow, switch-able main beam performance, array configuration is necessary for our purpose. The basic array antenna model consists of two parts, the element pattern, and the pattern of the array with the actual elements replaced by isotropic point sources, named array factor. The entire pattern of the array is the product of the element pattern and the array factor.

2.1 Array Factor

Consider a set of linear radiation sources as shown in figure 2-1

.
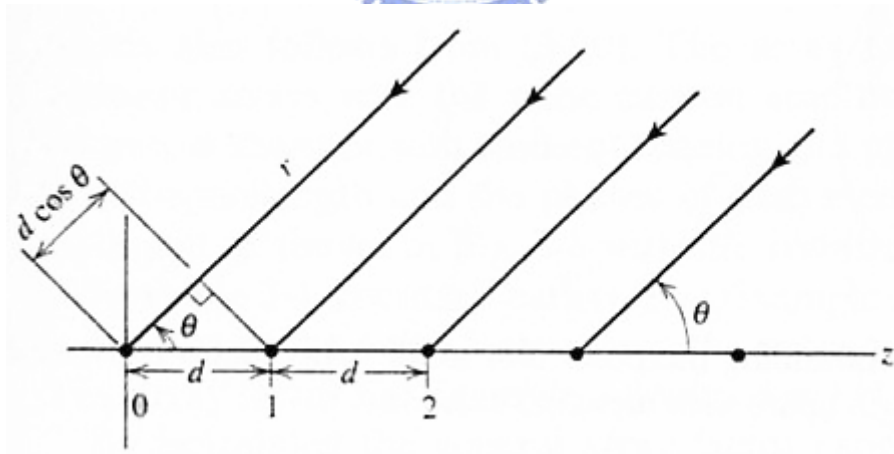
Fig. 2-1: equally spaced linear isotropic sources

The array elements are separated with d, and having a linear phase different α. The array factor of fig. 2-1 can be expressed as

$$AF = I_0 + I_1 e^{j\beta d \cos\theta} + I_2 e^{j\beta 2d \cos\theta} + \ldots = \sum_n I_n e^{j\beta n d \cos\theta} \qquad (2\text{-}1)$$

Where

$$I_n = A_n e^{jn\alpha} \qquad (2\text{-}2)$$

Define

$$\psi = \beta d\cos\theta + \alpha \qquad (2\text{-}3)$$

Then

$$AF = \sum_{n=0}^{N-1} A_n e^{jn\psi} \qquad (2\text{-}4)$$

Figure 2-2 shows the array factor pattern for an array to be constructed with four elements (N=4), uniformly excitation, equally spaced phase array (d= λ /2 and α= π /2).

(a)

$$|f(\psi)| = \left| \frac{\sin 2\psi}{4 \sin \frac{\psi}{2}} \right|$$

(b)

$$\theta_o = 120°$$

$$\beta d = \pi$$

$$\alpha = \frac{\pi}{2}$$
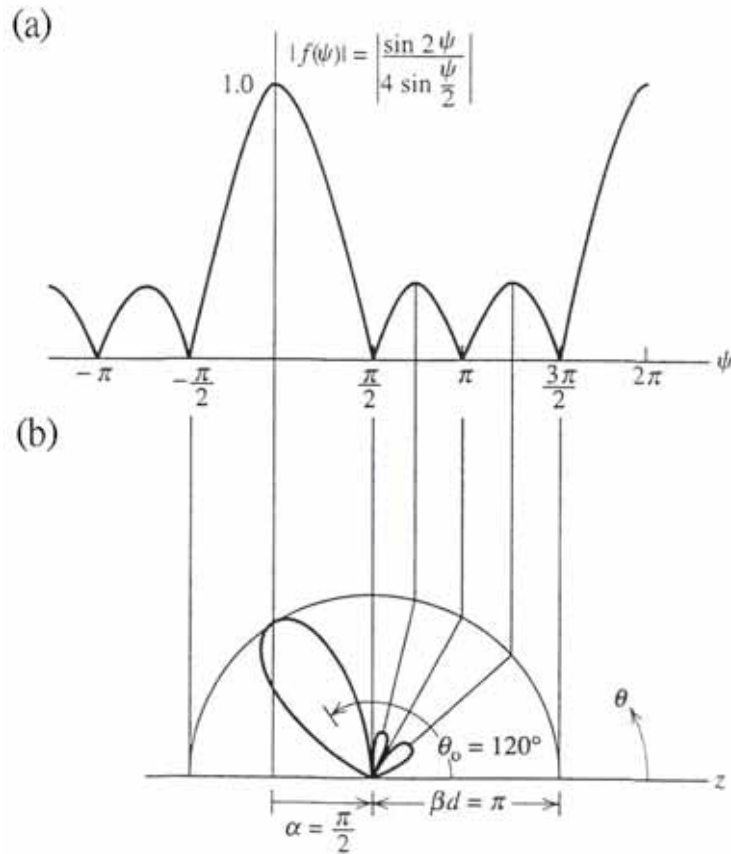
Fig. 2-2: array factor for N=4, d= λ/2 and α= π /2 array, and (a) universal pattern

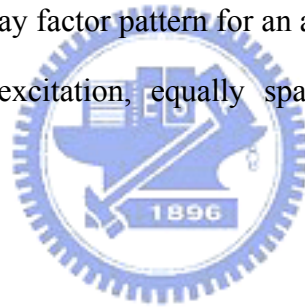*for N=4, (b) polar plot*

2.2 Phase Arrangement

According to the purpose of this thesis, the main beam of the array should be switched in 3 different directions. The antenna sub-array rows ought to be in phase for the center beam; for the symmetrical oblique beam, there are constant phase differences along the feeding point of the antenna row. Refer to figure 2-2, we spaced 5mm and set $60.43°$ ($= \beta d \tan 7.5°$) in phase difference between each antenna row feeding point to procure $7.5°$ oblique beam.

Chapter 3   Microstrip Antenna

Microstrip devices are layered structures with parallel conductors separated by thin dielectric films. For a single layer microstrip structure, a long-narrow-strip shape upper conductor forms a microstrip transmission line, a patch forms a microstrip antenna for certain frequency.

Microstrip antenna is the most common form of printed antennas. Printed antennas are popular for low cost, simple fabrication process, low profile, and can be easily combined with microwave circuits.

3.1 Theory of Microstrip Antenna

a.   transmission line model: [2, 3]

The simplest analytical description of a rectangular microstrip patch applies transmission line theory and models the patch as two parallel radiating slots. A rectangular microstrip antenna is expressed as an array of two radiating apertures as shown in figure 3-1 due to fringing fields at the edges. The fringing fields expend the effective length of the patch. Thus, the length of a half-wave patch is slightly less then a half wavelength in the dielectric substrate material. The region between conductors acts a half-wavelength transmission line with open-circuited at its ends.
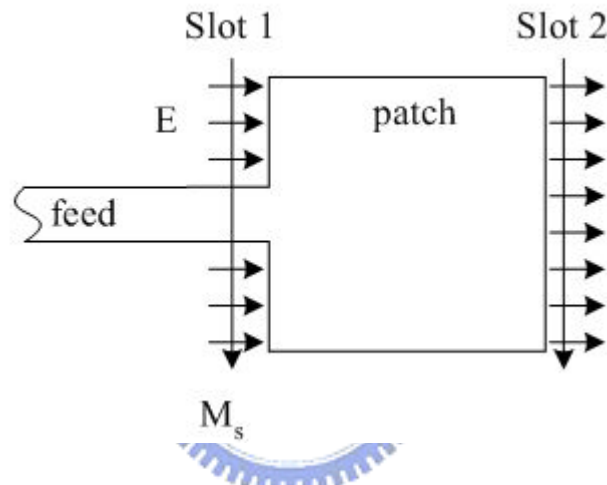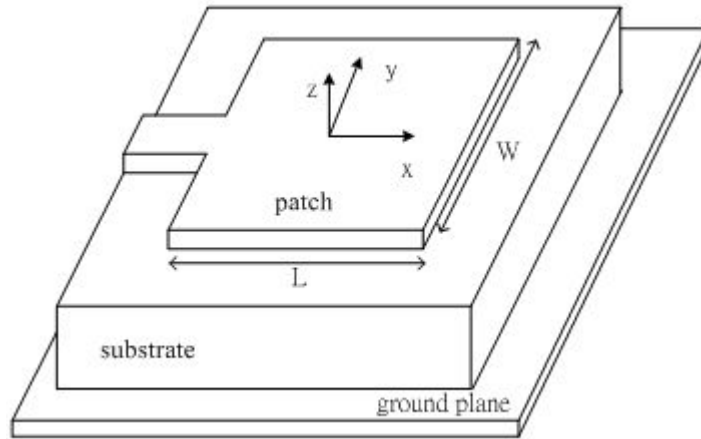
Fig. 3-1: The rectangular patch microstrip antenna

The advantage of transmission line model is simple; the resonant frequency is given by the formula (3-1). Fringing field should be considered in real would, which causes the extension of the effective length. The fringe factor q determines the accuracy of the resonant frequency, it is determined by measuring f_r for a rectangular patch on certain substrate and assumes that the same q for other patches of other sizes on the same substrate in the same frequency range.

$$f_r = q \frac{c}{2l\sqrt{\varepsilon_r}} \tag{3-1}$$

b. cavity model: [2, 3]

Even though the transmission line model is easy for use, there are still some drawbacks. The fringing effect must be determined with instinct, it omits field variations along the radiating edge, and it is not adjustable with the feeding effect. These drawbacks are vanished in the cavity model; the patch is viewed as a thin TM_z-mode cavity with conductor parallel planes and magnetic walls. The field between the patch and the ground plane is expanded in terms of a series of cavity resonant modes or eigenfunctions along with its eigenvalues or resonant frequencies associated with each mode. This is an approximate model, which causes none radiating power and forms reactive input impedance. For accuracy radiation calculating, loss and radiation must be taken into account by introducing loss tangent and more accomplished boundary condition.

3.2 Design of Microstrip Antennas

a. choose of substrates

There are two important parameters of substrate for fabricating microstrip antennas, dielectric constant and loss tangent. Higher dielectric constant minimize the size of microwave structures, but also reduce the bandwidth; similarly, larger lose tangent leads to lower radiation efficiency and more feeding lose.

In general, designers choose the thicker substrates with lower dielectric constant for higher radiation efficiency and wider bandwidth. Nevertheless, substrates with excessive thickness result in the excitation of surface wave, which decreasing the radiation efficiency.

Radiation pattern of microstrip antenna can be expressed as two radiating slot,

whether in transmission line model or in cavity model, as shown in figure 3-2. Note that the E-plane and the H-plane radiation pattern are different due to the different relative position of the magnetic current.
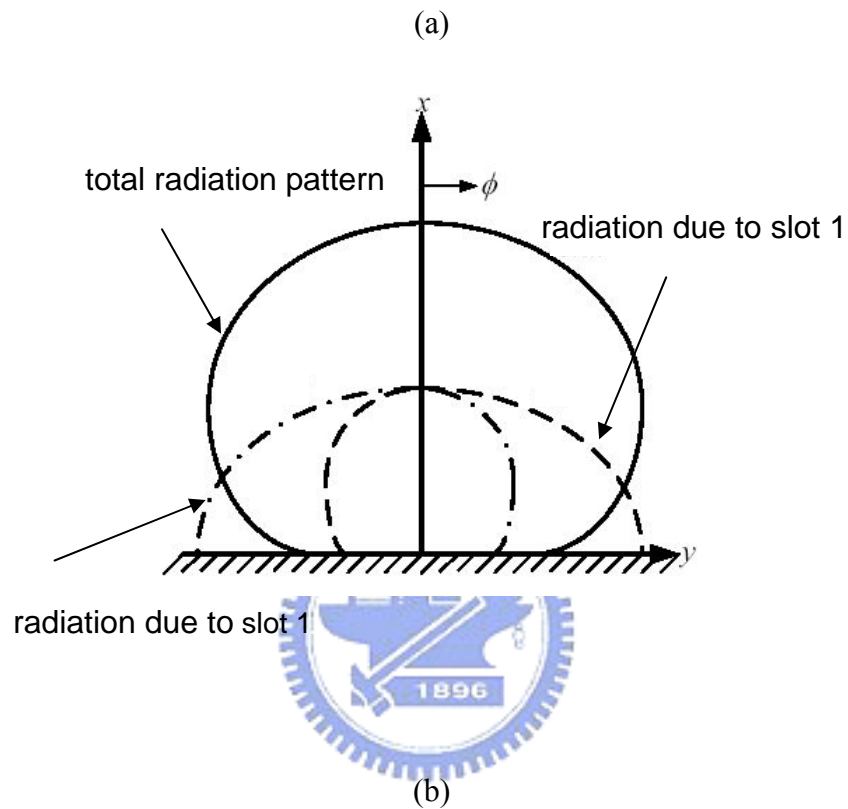
(a)

(b)

Fig. 3-2: radiation pattern of microstrip antenna, (a) E-plane, (b) H-plane

b. Feeding methodology

There are several typical feeding structures for microstrip antenna as shown in figure 3-3, [2];
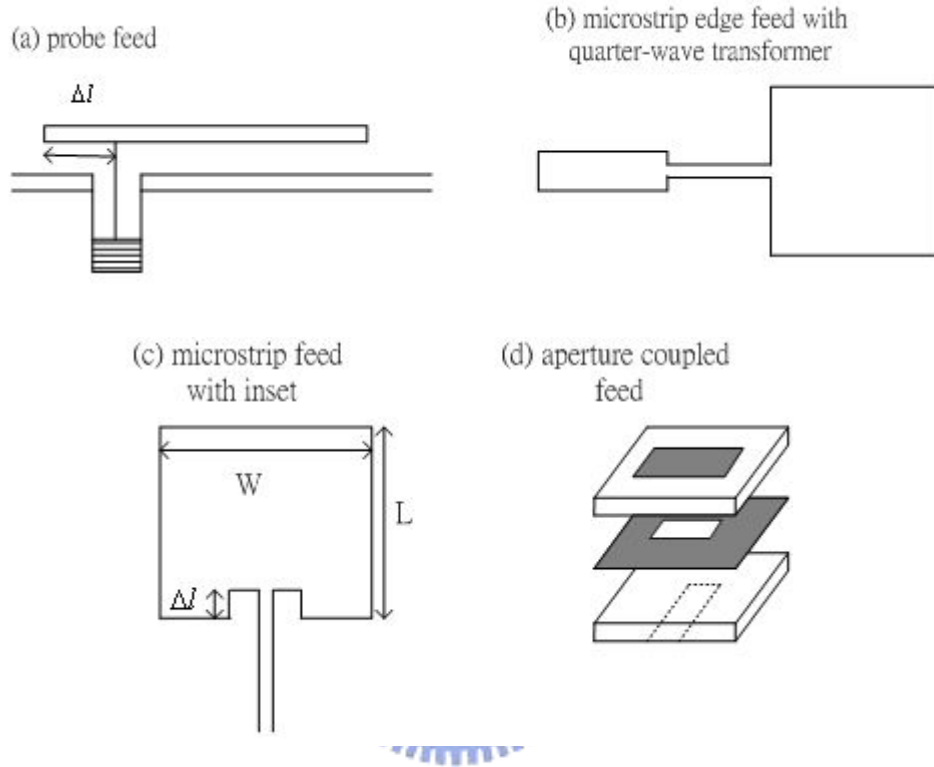

Fig. 3-3: feeding methodology

The basic rule to feed a microstrip line is to find an appropriate point for impedance matching. Typical input impedances at the edge of a resonant rectangular patch range from 100 to 400Ω. An approximate for the impedance of a resonant patch in situation of fig. 3-3 (a), and (c) is

$$Z_{in} = Z_A \cos \frac{\pi \Delta l}{L} \qquad (3-2)$$

$$Z_A = 90 \frac{\varepsilon_r^2}{\varepsilon_r - 1} (\frac{L}{W})^2 \qquad (3-3)$$

Where Z_A =input impedance of a resonant edge-fed patch

<center>*Δl =length inset or from the edge*</center>

For structure as in fig 3-3 (b), a quarter-wave transformer matching section translates the input impedance Z_A to the characteristic impedance Z_0 for the transmission line of the system. The lower substrate carrying the feed of aperture-coupled feed structure shown in fig. 3-3 (d) can be of high dielectric constant to enhance constraint of fields to the feed lines and the upper substrate can be of low dielectric constant to improve radiation.

In the thesis, microstrip antenna is fed in series to form a sub-array row, the connecting transmission lines should be chosen narrow for not to disturb the fields in the radiating slots.

In transmission line model (as shown in figure 3-4) [4,5], the radiating slot of the two port series fed microstrip patch element is modeled as a conductance G and a susceptance B in parallel, two additional reactances X_1 and X_2 are supplementary component indicating the step in width between feeding line and patch.
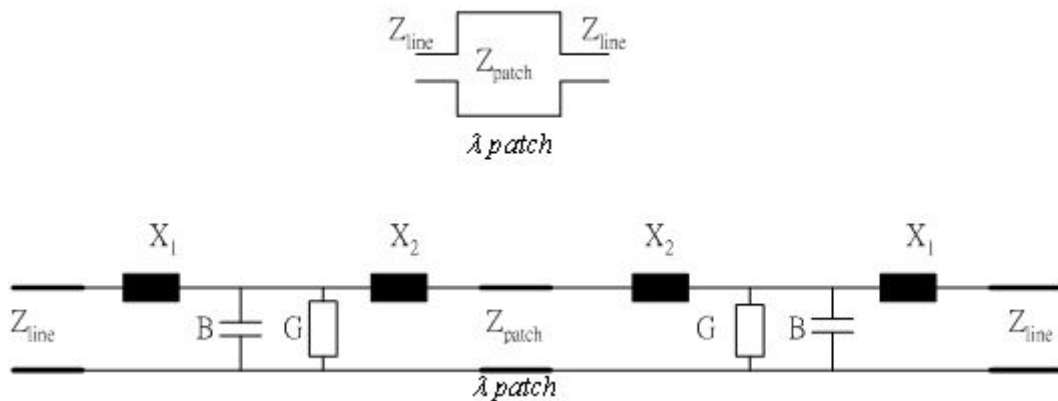
<center>*Fig. 3-4: transmission line model for two port microstrip antenna*</center>

For a series fed microstrip antenna row, the radiating patches are resonant so that the input line to a patch is matched if the output line is terminated. The phases of

the radiation sources can be controlled by selection of the position s of the patches on the row, for broadside radiation in this thesis, the patch elements are separated with half-wavelength to generate in phase excitation.

c. Design and measurement of microstrip antenna

The substrate RT-Duroid 5880 ($\varepsilon_r = 2.2$, thickness=0.127mm) has been chosen, this substrate is well suited for fabrication of microstrip antennas because of its low loss and uniform characteristics.

Patch elements are simulated with Zeland Software IE3D, the microstrip fed square patch shown in figure 3-5 is simulated and the result is shown in figure 3-6.
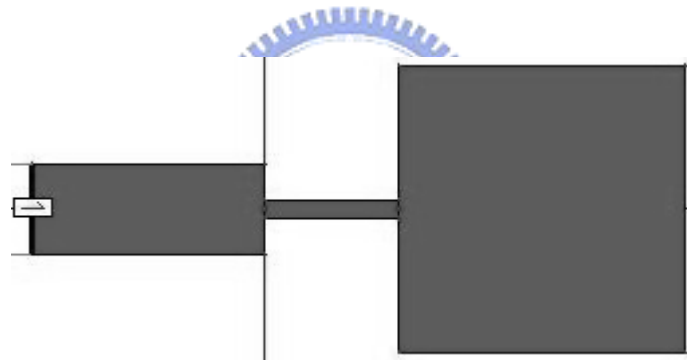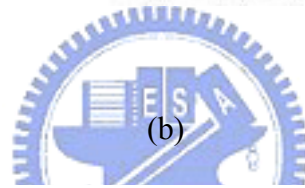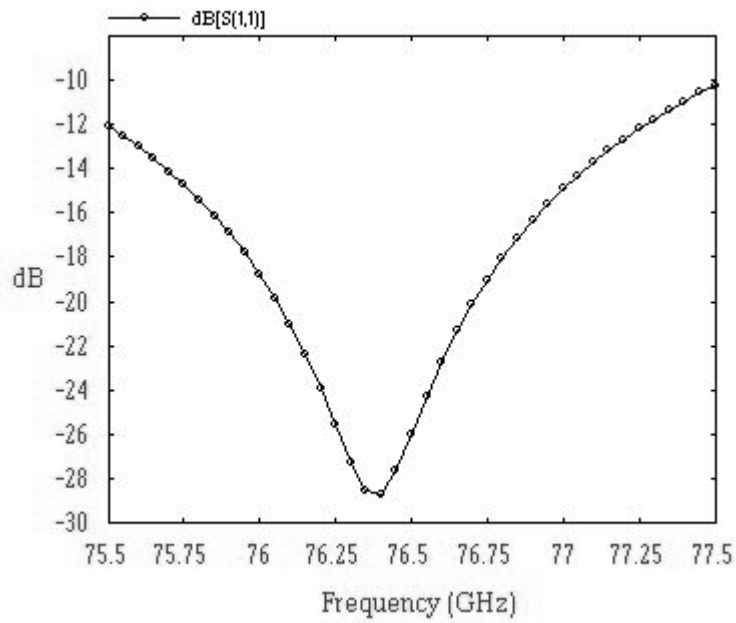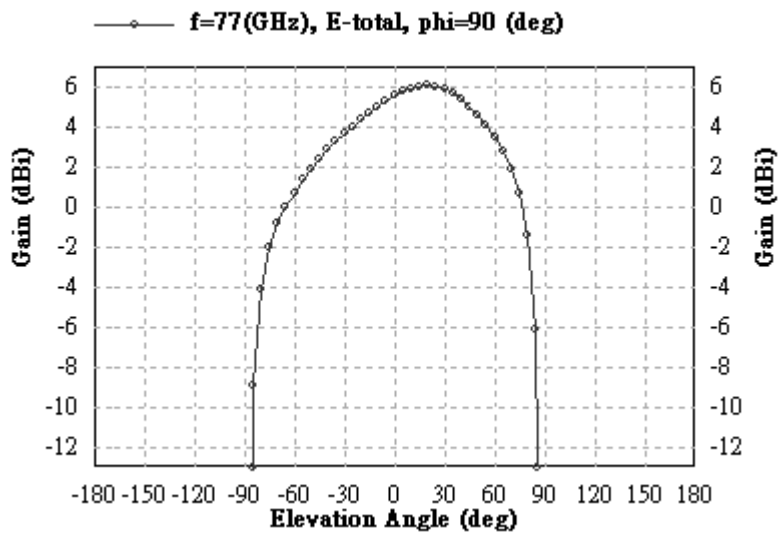

*Fig. 3-5: microstrip fed square patch*

(a)

(b)

Elevation Pattern Gain Display

3dB beamwidth=60°

*Fig. 3-6: simulation of patch antenna, (a) return loss and (b) pattern*

Owing to the limitation of computer calculating efficiency, it takes lots of time to simulate array structures containing over 10 elements. A compromise is made by calculating array pattern with array factor and the pattern of the single element. Based on the result of the calculation, 32 elements are needed to form a main beam narrower then 5° as the objective of this thesis. (Figure 3-7 shows the calculated patterns for linear array composed with 2, 4, 8, 16, 32 elements, respectively)
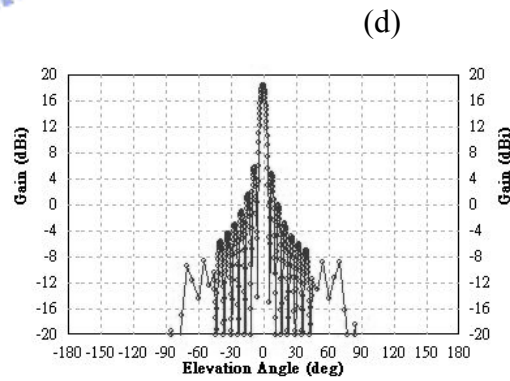
(a)
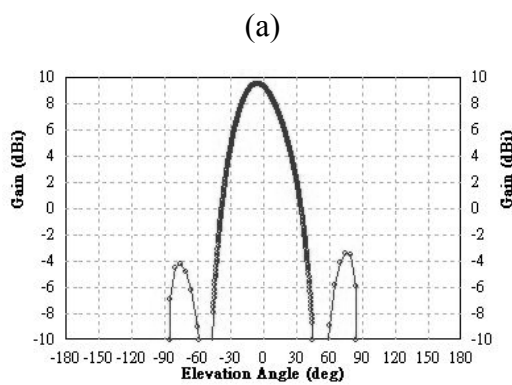
2 elements, 3dB beamwidth=24.3°

(b)
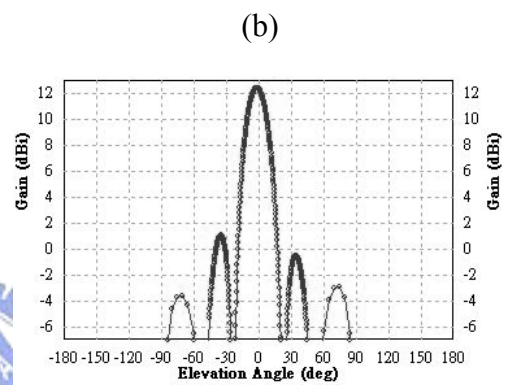
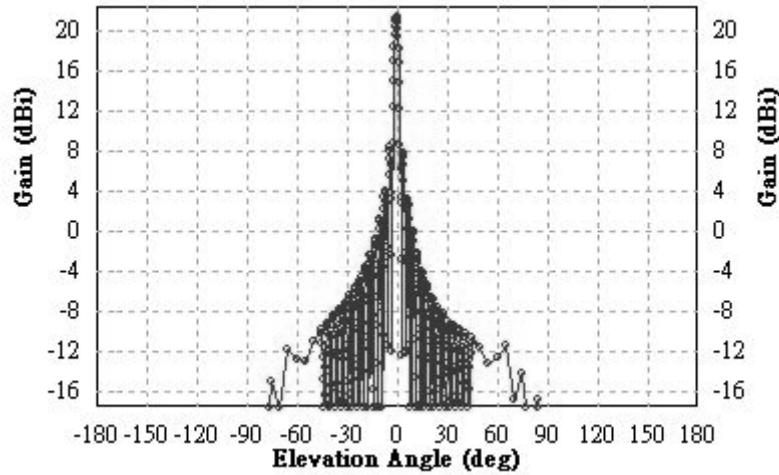4 elements, 3dB beamwidth=10.9°

(c)
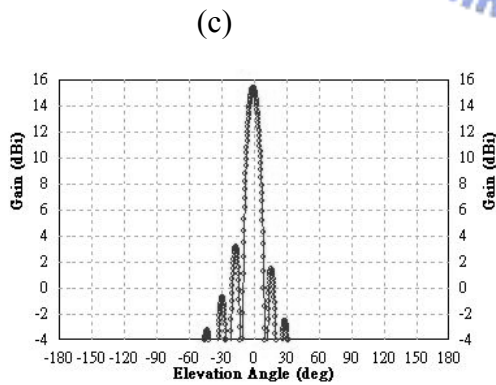
8 elements, 3dB beamwidth=5.1°

(d)

16 elements, 3dB beamwidth=4.99°

(e)

32 elements, 3dB beamwidth=2.5°

Fig. 3-7: calculating pattern of linear array with (a) 2 elements, (b) 4 elements, (c) 8 elements, (d) 16 elements, (e)32 elements,

In virtue of the high operating frequency, the size of the antenna are sensitive to resonating frequency, hence, the antennas are fabricated by professional PCB manufacturer to obtain a precise fabricating process.

The return loss measurement is performed with Agilent 8510 system and Anritsu test feature (as shown in figure 3-8), and the pattern is measured with the spectrum analyzer and custom made carrier, the measuring signal is generated at 38GHz and doubled to 76GHz by the UMS multiply power amplify (the pattern measuring system is illustrated in figure 3-9).
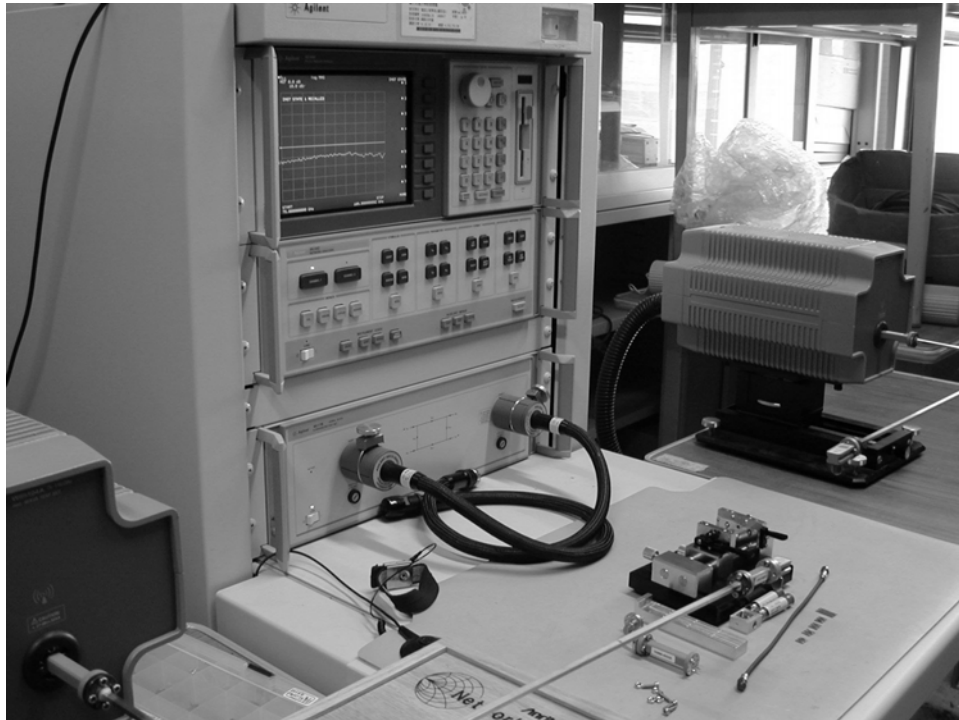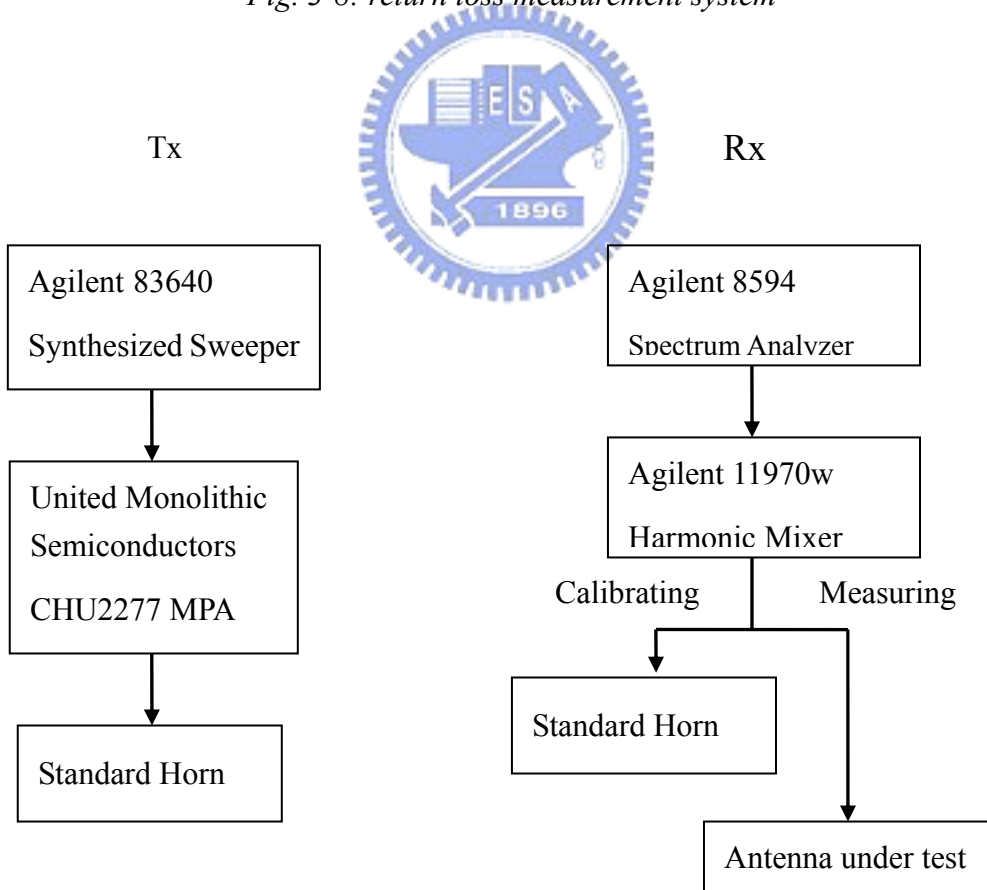
Fig. 3-8: return loss measurement system

Tx   Rx

Agilent 83640 Synthesized Sweeper	Agilent 8594 Spectrum Analyzer

United Monolithic Semiconductors CHU2277 MPA	Agilent 11970w Harmonic Mixer

Calibrating   Measuring

Standard Horn	Standard Horn

Antenna under test

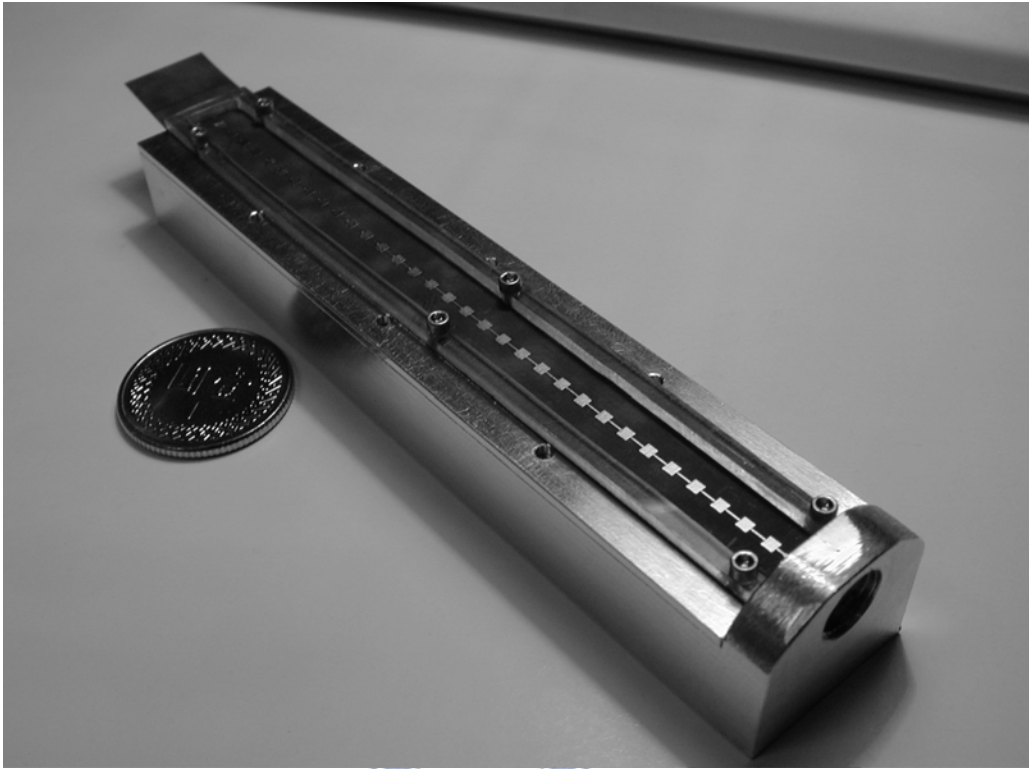*Fig. 3-9 (a): pattern measuring system*

Fig. 3-9 (b): custom made carrier

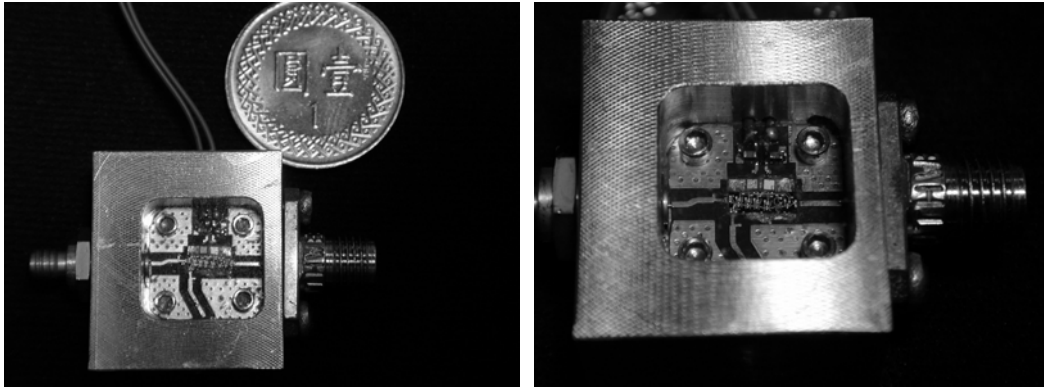*Fig. 3-9 (c): close-up photo of the connector*

Fig. 3-9 (d): UMS MPA set

The geometric structure of the row-array is shown in figure 3-11. Measurement of return loss and pattern are depicted in figure 3-12 and figure 3-13, the pattern shows approximate 4° 3-dB beamwidth for the main beam and the gain is about 12.53 dBi at 76.0GHz.
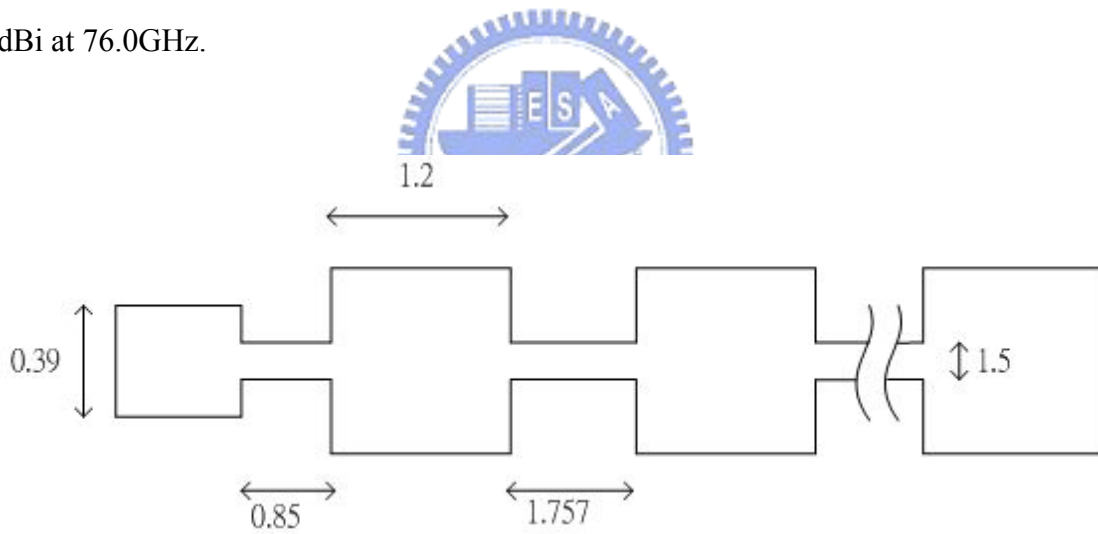

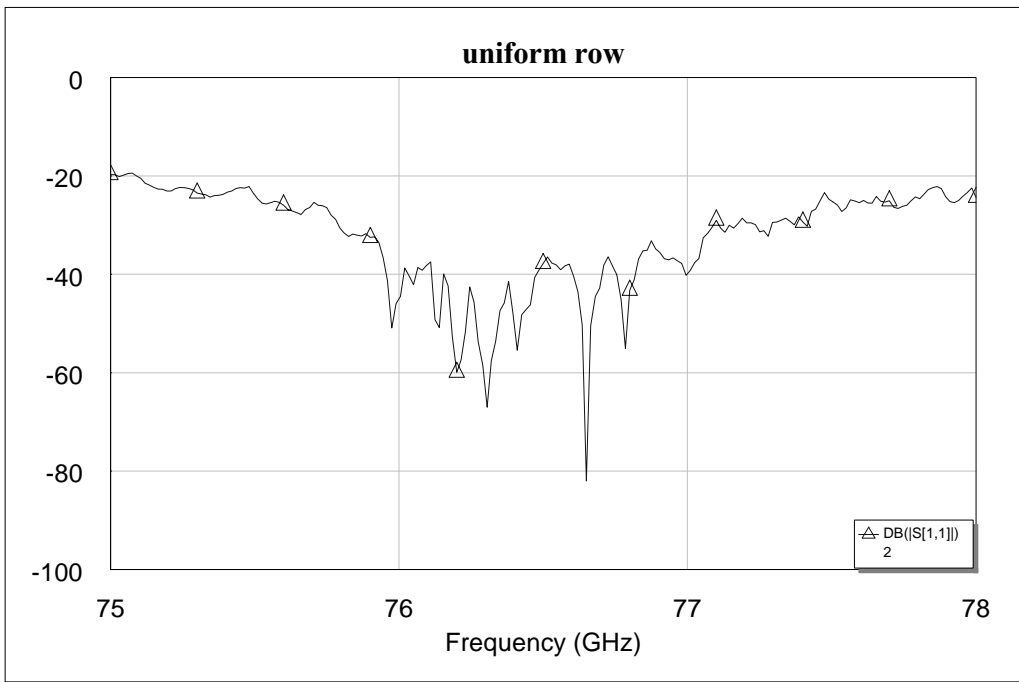*Fig. 3-11: uniform series fed array (dimensions in mm)*

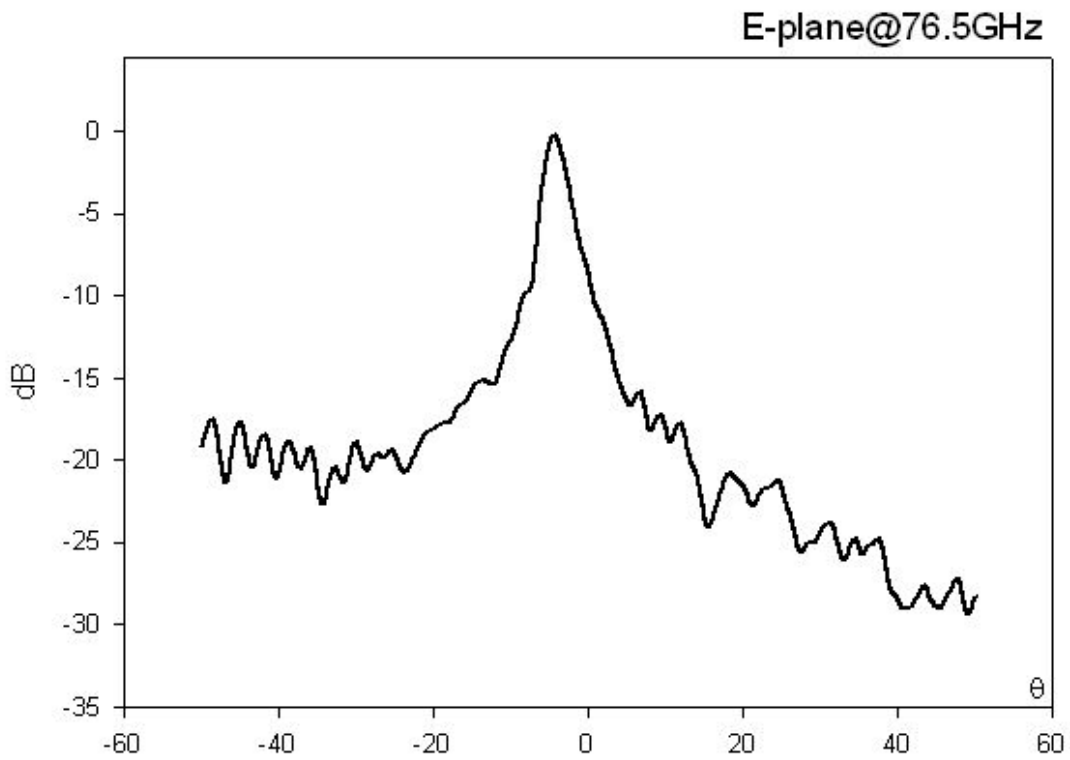*Fig. 3-12: measurement of return loss of the series fed array*

Fig. 3-13: E-plane pattern of the series fed array

The pattern above implies the defect of high side lobe level. We set a simulation with the linear array structure by Ansoft HFSS, verifying the assumption in figure 3-14. The simulation result shows the side lobe level is 8dB, which is not acceptable.
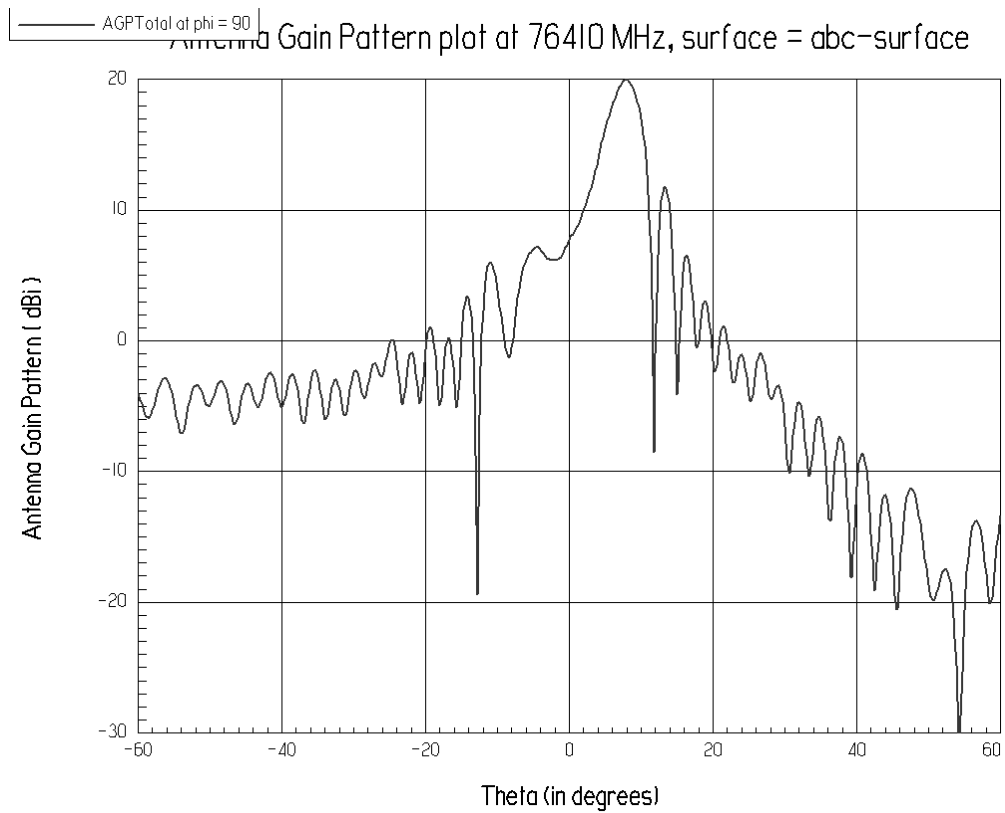

Fig. 3-14: simulated E-plane pattern

Due to the defect of high side lobe, tapered aperture is considered for array component, and an open stub is added at the end of array, instead of trimming the last element, to preserve the characteristic of symmetry. The added stub ought to be a quarter-wave in length, which keeps the correct wave from to excite broadside pattern, the relationship between pattern and the length of added stub is shown in figure 3-15.
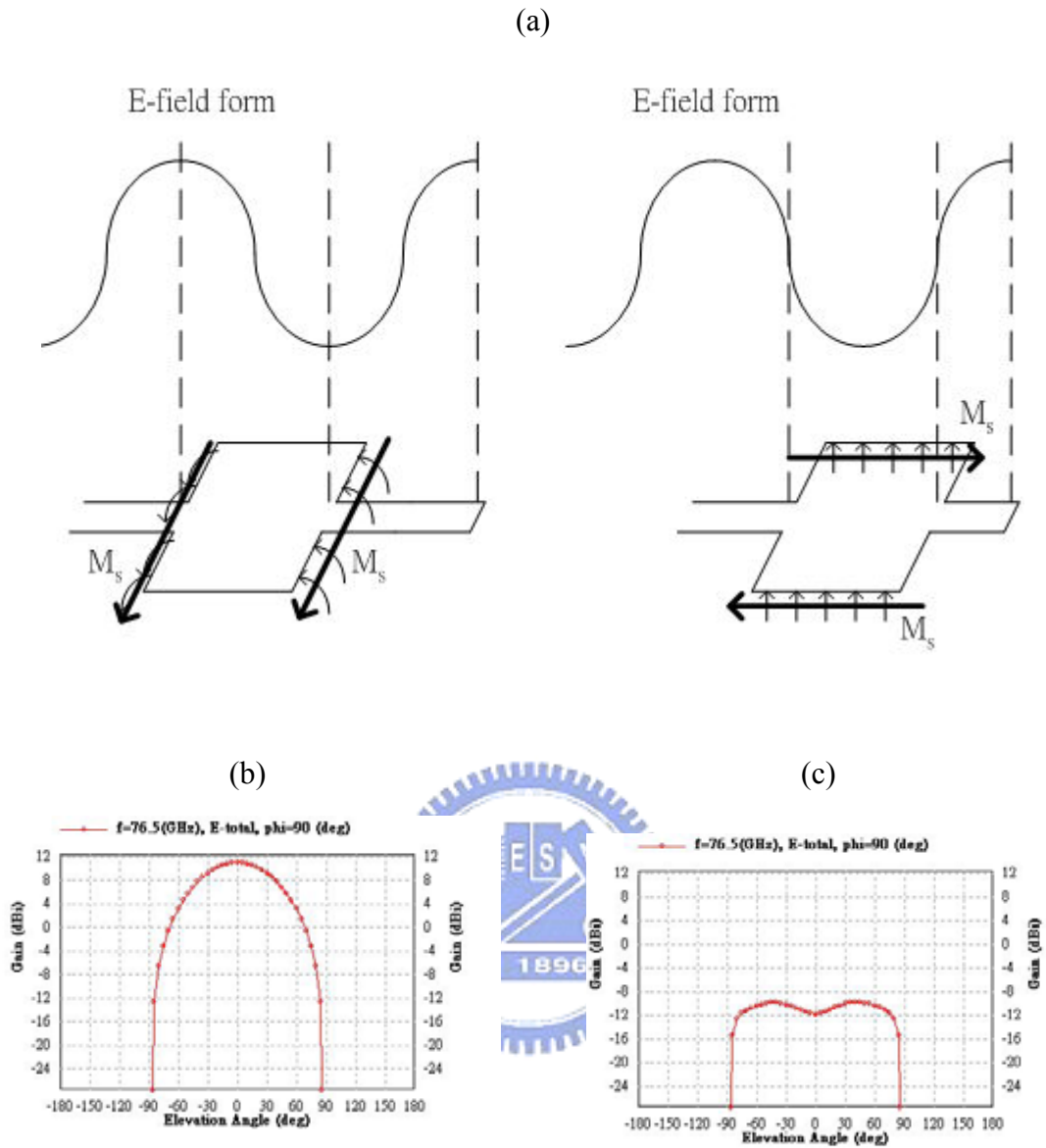
E-field form   E-field form

(b)   (c)

Fig. 3-15: demonstrate of stub effect: (a) magnetic current excitation, and E-plane

pattern of 3 elements array ended by (b) two situation, and (c) quarter-wave stub

The tapered array is composed with 33 patch elements, table 3-1 and figure 3-16 shows the pattern of different taper setting, and the simulation result of the chosen configuration (S15) is shown in figure 3-17.

No.	P1 & P33	P2 & P32	P3 & P31	P4 & P30	P5 & P29	P6 & P28	P7 & P27	P8 & P26	P9 & P25	P10 & P24	P11 & P23	P12 & P22	P13 & P21	P14 & P20	P15 & P19	P16 & P18	P17
S5	0.9	0.9	0.9	1.1	1.1	1.1	1.1	1.1	1.3	1.3	1.3	1.3	1.3	1.6	1.6	1.6	1.6
S9	0.8	0.8	0.9	0.9	1.0	1.0	1.1	1.1	1.3	1.3	1.5	1.5	1.7	1.7	1.8	1.8	1.9
S10	0.9	0.9	0.9	1.1	1.1	1.1	1.1	1.1	1.5	1.5	1.5	1.5	1.5	1.7	1.7	1.7	1.7
S15	0.7	0.7	0.7	0.9	0.9	0.9	1.3	1.3	1.3	1.6	1.6	1.6	1.6	1.7	1.7	1.7	1.7

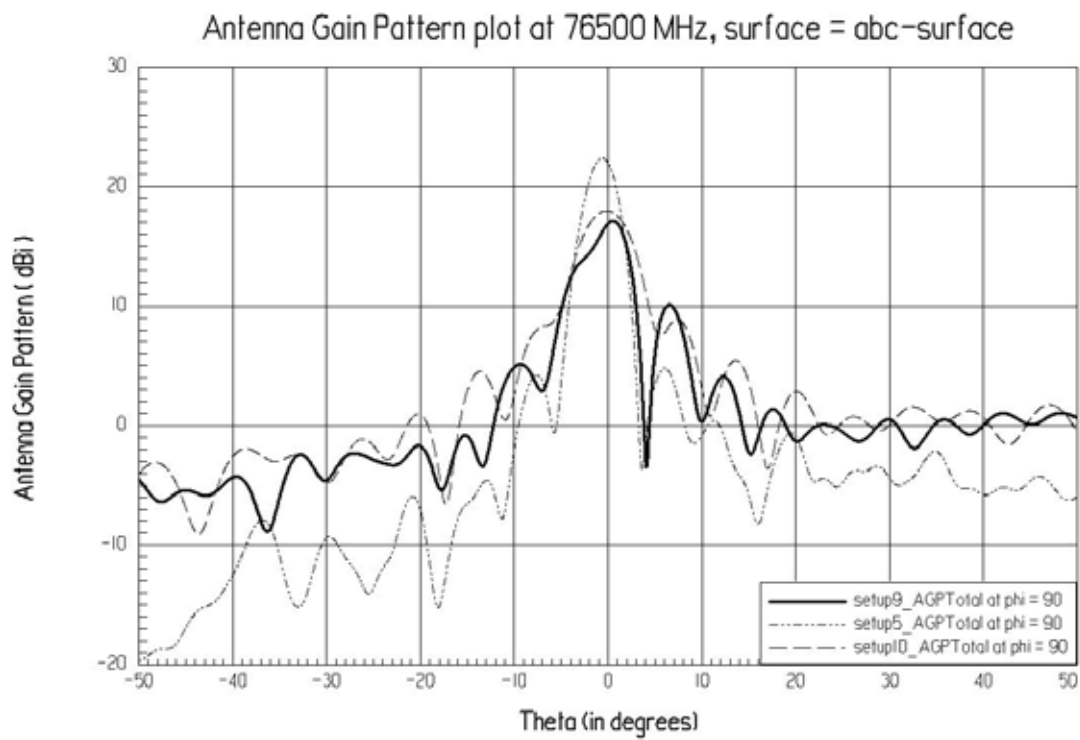(Dimensions in mm)

Table 3-1: setting of tapered antennas

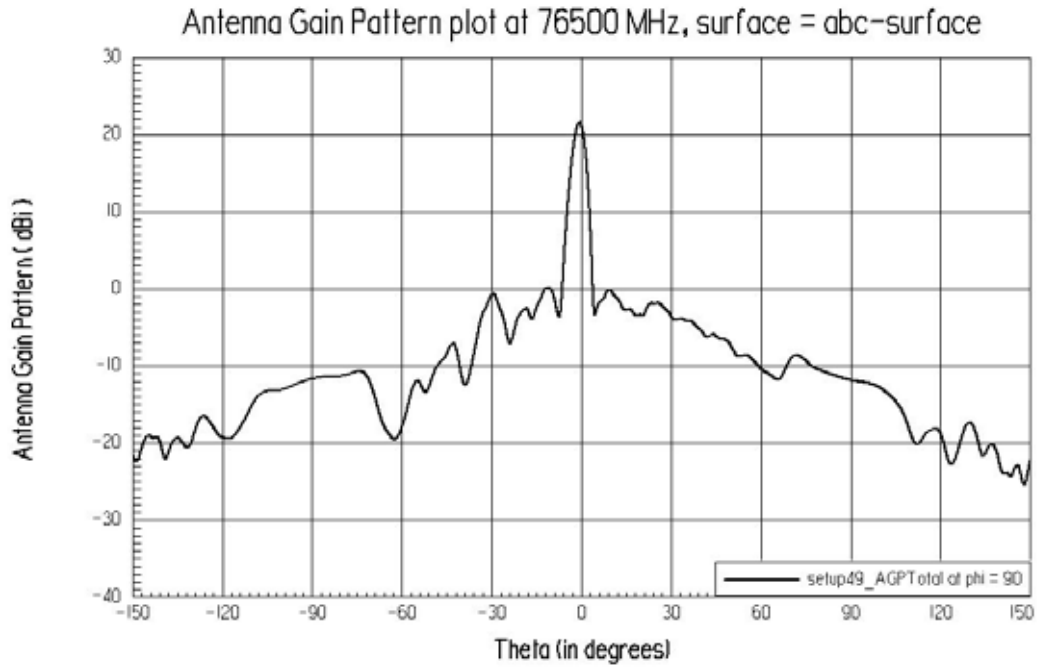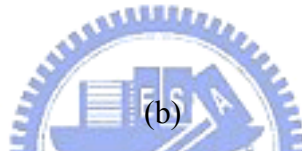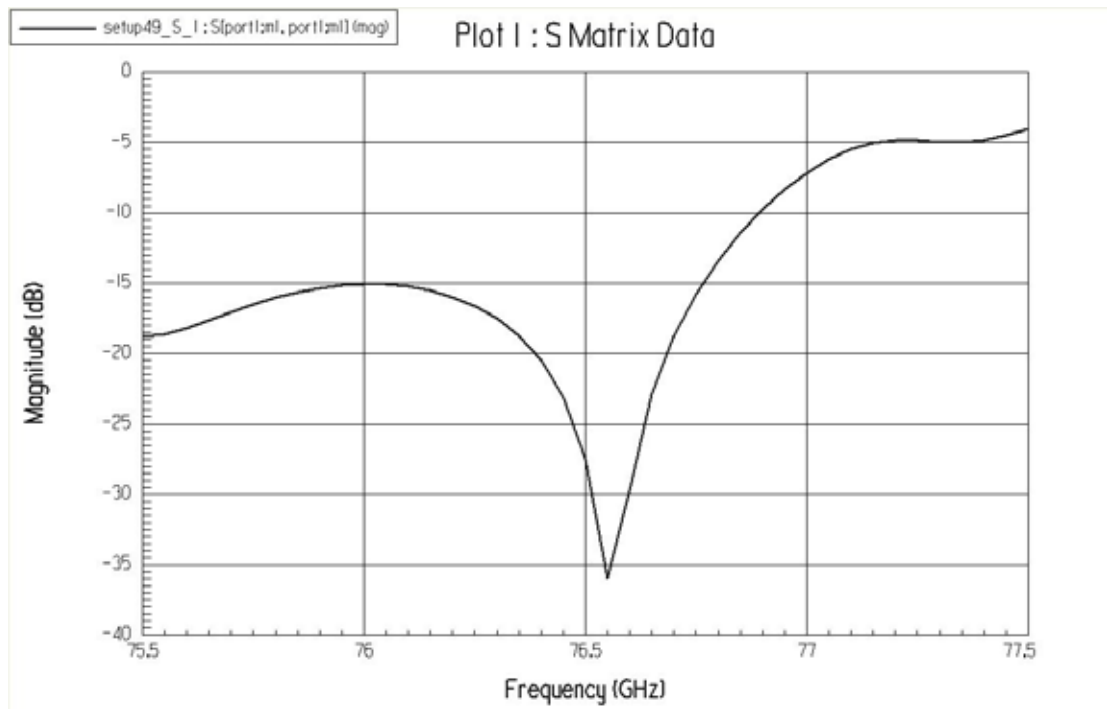*Fig. 3-16: E-plane pattern of S5, S9 and S10 tapered antennas*

(a)

(b)

Fig. 3-17: simulated (a): return loss and (b): E-plane pattern of tapered array

The measurement results are shown in figure 3-18. As shown in figure 3-18, side

lobes of the tapered array are below then 15dB, which is slightly higher then the simulation, but still be acceptable, and the antenna gain is approximately 16dBi.
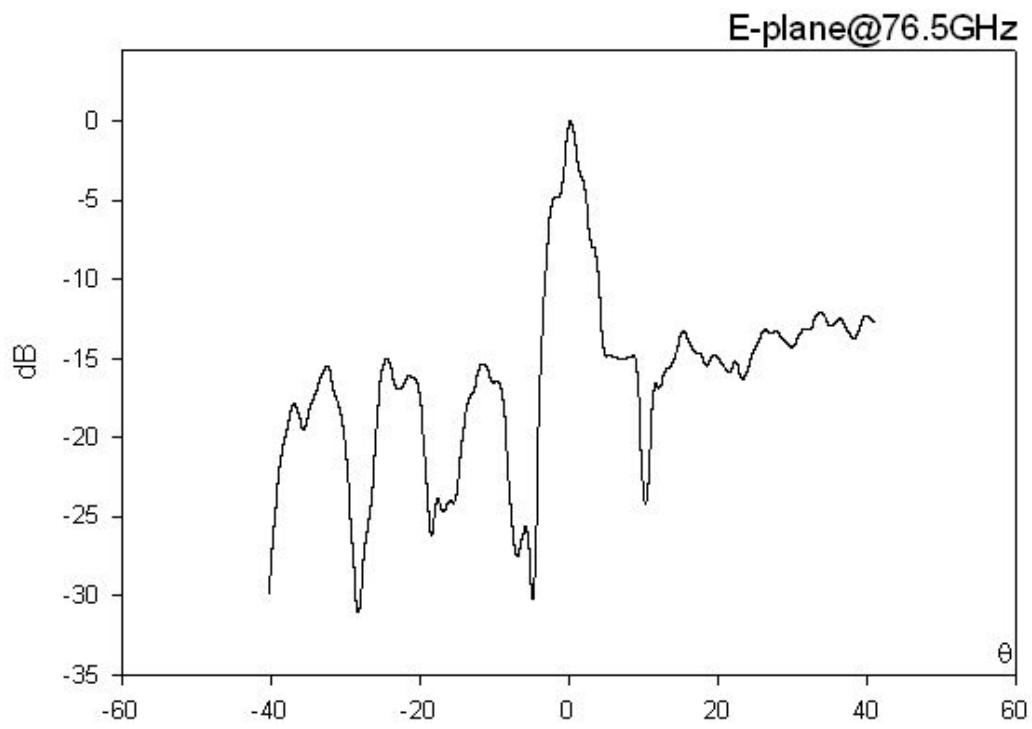
(a)
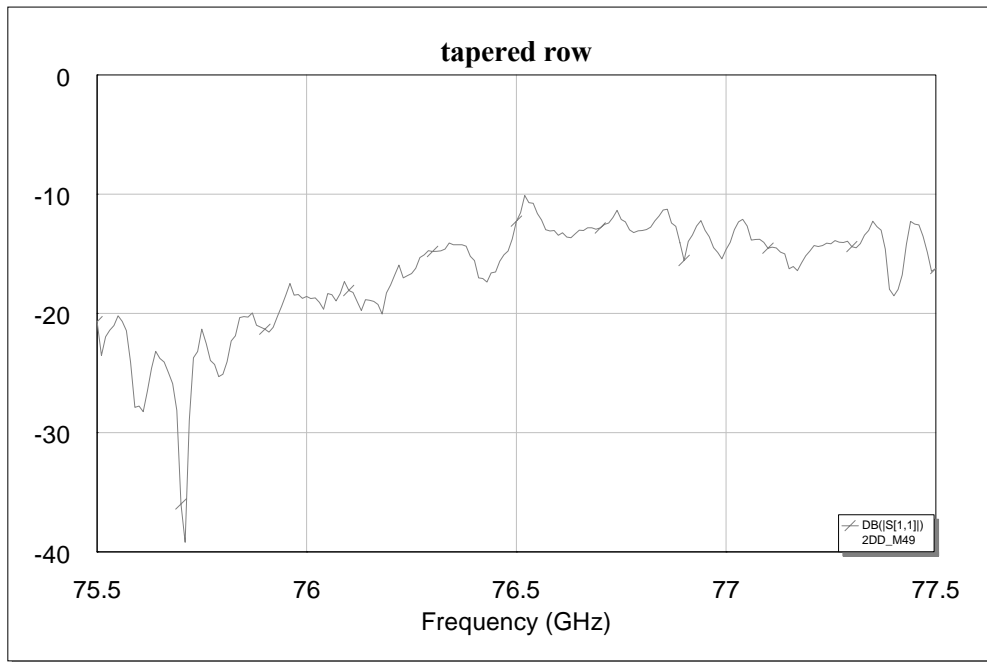
tapered row

(b)

Fig. 3-18: measurement of the tapered antenna, (a) return loss and (b) E-plane

pattern

Chapter 4. Rotman Lens

Rotman lens is useful in variety of electronically steered radar applications. It provides a simple geometry structure for beam switching/steering application by calculating the path different from input ports to output ports. Figure 4-1 depicts the function of Rotman lens, signals fed in I_C, I_L, and I_R result in beams marked with R_C, R_L, and R_R, respectively.
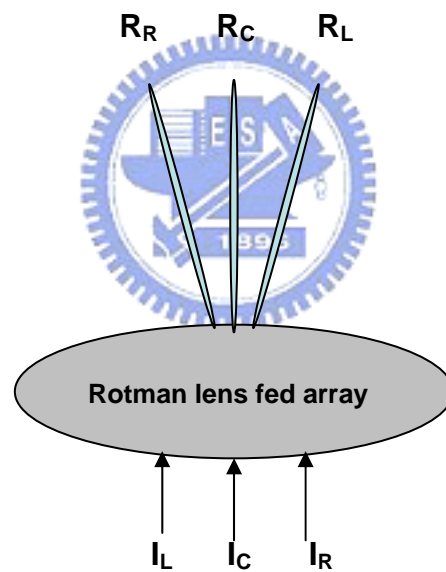

Fig. 4-1: brief describe of Rotman lens

4.1 Foundation of Rotman Lens

A typical lens design is initiated by solving the Rotman equations [6]. The

geometrical pattern of the lens is described by equations with design parameters, e.g.

focal point, off-axis focal point, output beam angle, etc. However, the design

equations do not specify the difference of propagation characteristic for microstrip

line and parallel waveguide. This thesis proposes modified Rotman lens equations,

consider lens as figure 4-2, two symmetrical off-axis focal point F_1 and F_2, and one

on-axis focal point G are points of perfect focus for radiation at angles to the axis of

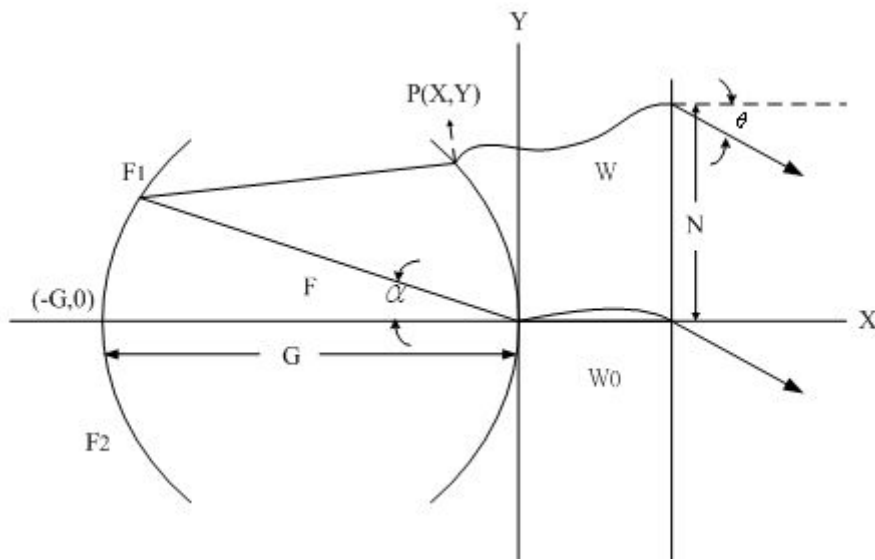$+\beta$, $-\beta$, and $0°$, respectively.

Fig. 4-2: Rotman lens geometry

Modified Rotman lens equations:

Consider general rays from focal points:

$$\beta_1 \cdot (\overrightarrow{F_1 P}) + \beta_2 \cdot W + \beta_2 \cdot N \sin\theta = \beta_1 \cdot F + \beta_2 \cdot W_0 \, l \qquad (4\text{-}1)$$

$$\beta_1 \cdot (\overrightarrow{F_2 P}) + \beta_2 \cdot W - \beta_2 \cdot N \sin\theta = \beta_1 \cdot F + \beta_2 \cdot W_0 \qquad (4\text{-}2)$$

$$\beta_1 \cdot (\overrightarrow{GP}) + \beta_2 \cdot W = \beta_1 \cdot F + \beta_2 \cdot W_0 \qquad (4\text{-}3)$$

Where β1=propagation constant of lens region

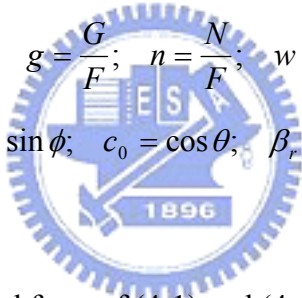β2=propagation constant of microstrip line region

$$(\overrightarrow{F_1P})^2 = F^2 + X^2 + Y^2 + 2FX\cos\phi + 2FY\sin\phi \qquad \text{(4-4)}$$

$$(\overrightarrow{F_2P})^2 = F^2 + X^2 + Y^2 + 2FX\cos\phi + 2FY\sin\phi \qquad \text{(4-5)}$$

$$(\overrightarrow{GP})^2 = (G+X)^2 + Y^2 \qquad \text{(4-6)}$$

These equations are derived directly from the geometry of figure 4-2, and then define a set of normalized parameters relative to the focal length F:

$$x = \frac{X}{F}; \quad y = \frac{Y}{F}; \quad g = \frac{G}{F}; \quad n = \frac{N}{F}; \quad w = \frac{W-W_0}{F}$$

$$a_0 = \cos\phi; \quad b_0 = \sin\phi; \quad c_0 = \cos\theta; \quad \beta_r = \frac{\beta_2}{\beta_1}$$

Combining the normalized form of (4-1) and (4-4), (4-3) and (4-6)

$$(\frac{\overrightarrow{F_1P}}{F})^2 = 1 + x^2 + y^2 + 2a_0x - 2b_0y = (1 - \beta_r w - \beta_r n c_0)^2 \qquad \text{(4-7)}$$

$$(\frac{\overrightarrow{GP}}{F})^2 = (g+x)^2 + y^2 = (g - \beta_r w)^2 \qquad \text{(4-8)}$$

Eq. (4-7) could be transferred to present the relation of (4-2) and (4-5) if n is replaced by −n, and y is replaced by −y. Then,

$$y = \frac{\beta_r n c_0}{b_0}(1 - \beta_r w) \qquad \text{(4-9)}$$

$$x^2 + y^2 + 2a_0\,x = (\beta_r\,w)^2 + (\beta_r\,n\,c_0)^2 - 2\beta_r\,w \qquad (4\text{-}10)$$

(4-8), (4-9) and (4-10) give the relation between w and n.

$$aw^2 + bw + c = 0 \qquad (4\text{-}11)$$

Where

$$a = \beta_r{}^2 - \frac{\beta_r{}^4\,c_0{}^2\,n^2}{b_0{}^2} - \beta_r{}^2\,(\frac{g-1}{g-a_0})^2 \qquad (4\text{-}12)$$

$$b = \frac{2g\,\beta_r(a_0-1)}{g-a_0} - \frac{\beta_r{}^3\,c_0{}^2\,n^2\,(g-1)}{(g-a_0)^2} + \frac{2\beta_r{}^3\,c_0{}^2\,n^2}{b_0{}^2} \qquad (4\text{-}13)$$

$$c = \frac{g\,(\beta_r\,c_0\,n)^2}{g-a_0} - \frac{\beta_r{}^2\,c_0{}^2\,n^2}{b_0{}^2} - \frac{(\beta_r\,c_0\,n)^4}{4(g-a_0)^2} \qquad (4\text{-}14)$$

w can be computed as a function of n from (4-11) to (4-14) for designate values of parameters.

4.2 Lens Contour Calculation

Rotman lens equations have been indicated that design parameters affect the lens contour obviously (as mentioned in [7]). Equations of modified Rotman lens derived above are calculated with Matlab, the relations between lens contour and the parameters are shown as follow:
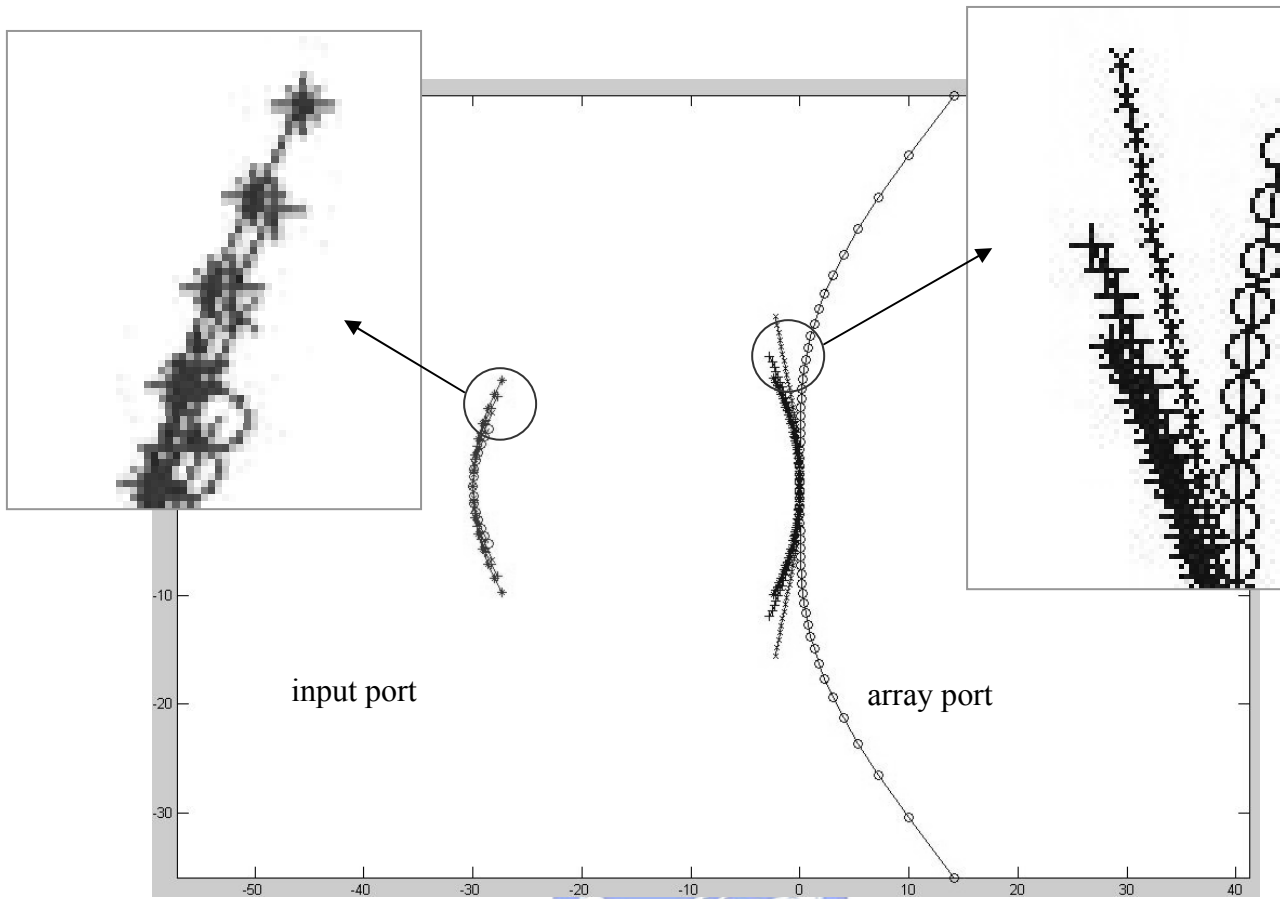
Fig. 4-3: effect of focal angle

Figure 4-3 shows the effect of the focal angle α, increasing α opens the input port and closes the array port (α =5°, 7°, 9°, and 11° for o mark, x mark, + mark and * mark, respectively, with all other variables fixed).

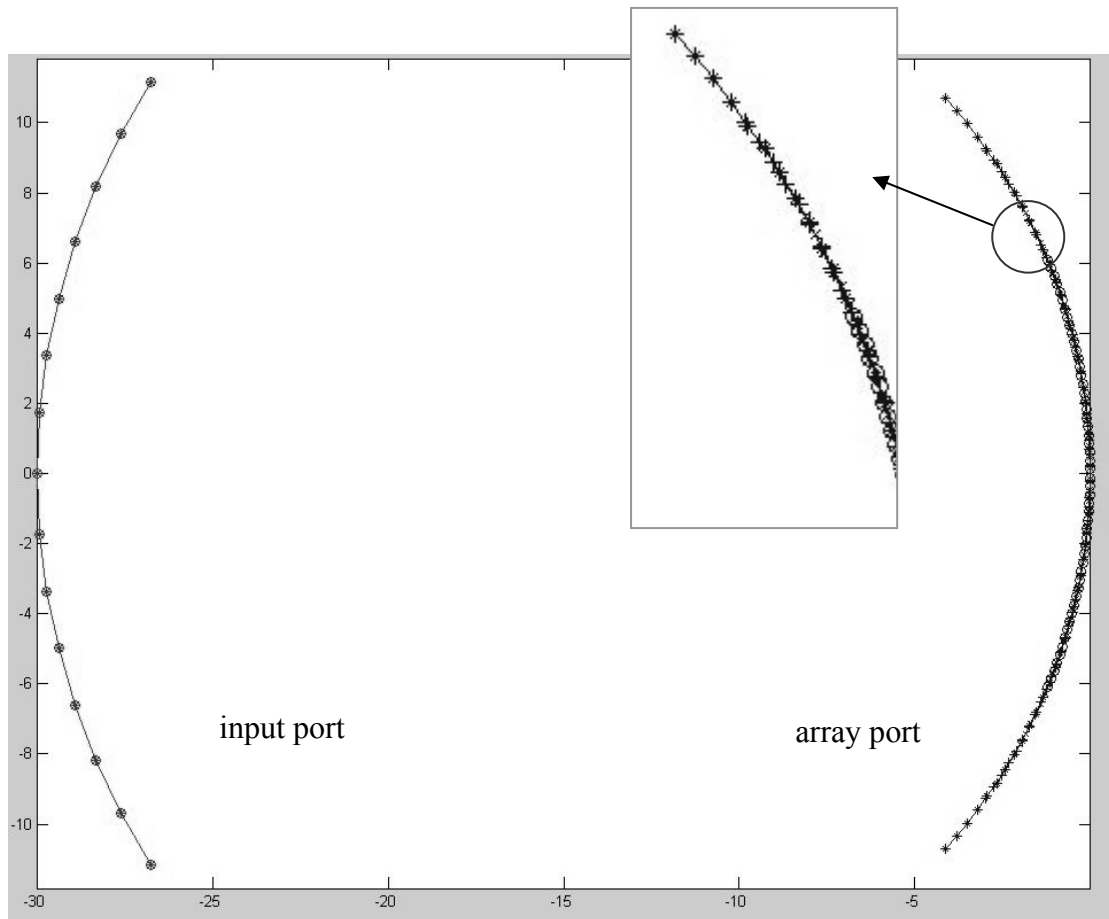*Fig. 4-4: effect of beam angle*

The effect of beam angle β is shown in figure 4-4, for β is 5° (with o mark), 7° (with x mark), 9° (with + mark), and 11° (with * mark), the input ports keep unchanged and the width of array port contour is reducing.
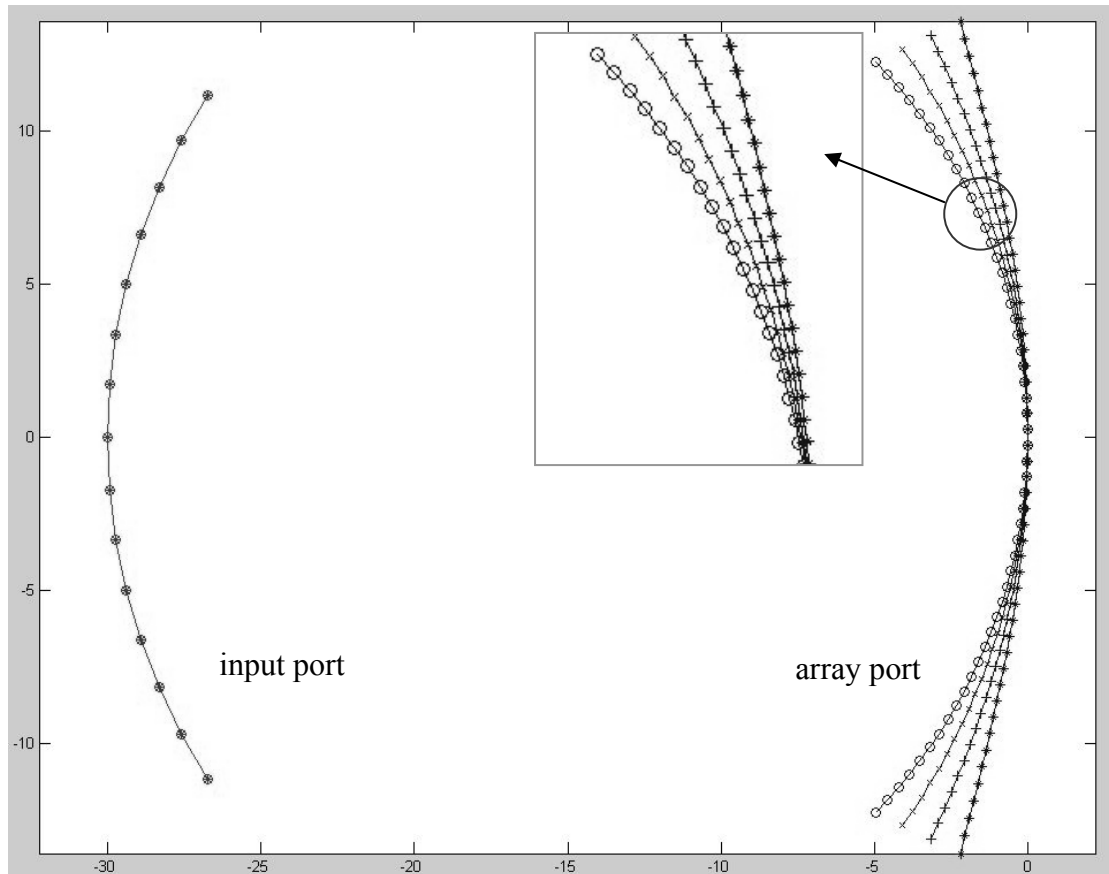
Fig. 4-5: effect of focal ratio

When the focal ratio g (=G/F, G is fixed) changes, only the array port contour follows, figure 4-5 depicts the result of changing g, increasing g opens the input port contour (g=1.01, 1.02, 1.03, and 1.04 for o mark, x mark, + mark and * mark, respectively, with all other parameters unchanged).

4.3 Design of Modified Rotman Lens

To verify the design of modified Rotman lens, a simple 3 input ports (3 available beam directions) to 4 output array ports lens is made. The lens fed four microstrip

sub-arrays, each content a power divider and a 3-elements microstrip series fed row (illustrated in figure 4-6). Power dividers are participated for earning space for microstrip meander line. The measurements of the antenna sub-array are shown in figure 4-7 and figure 4-8.
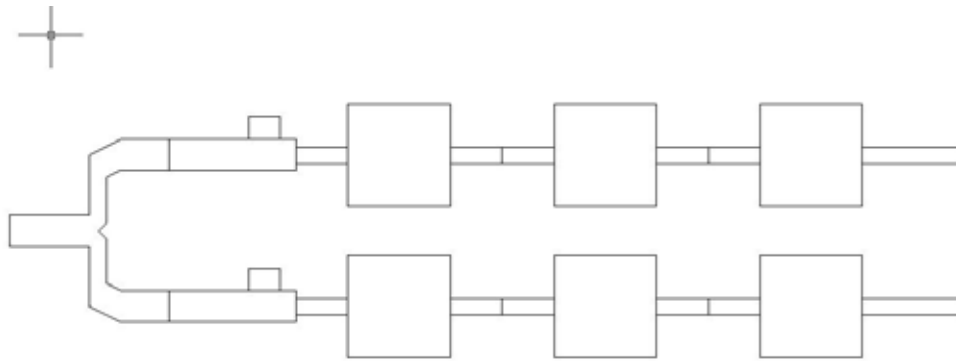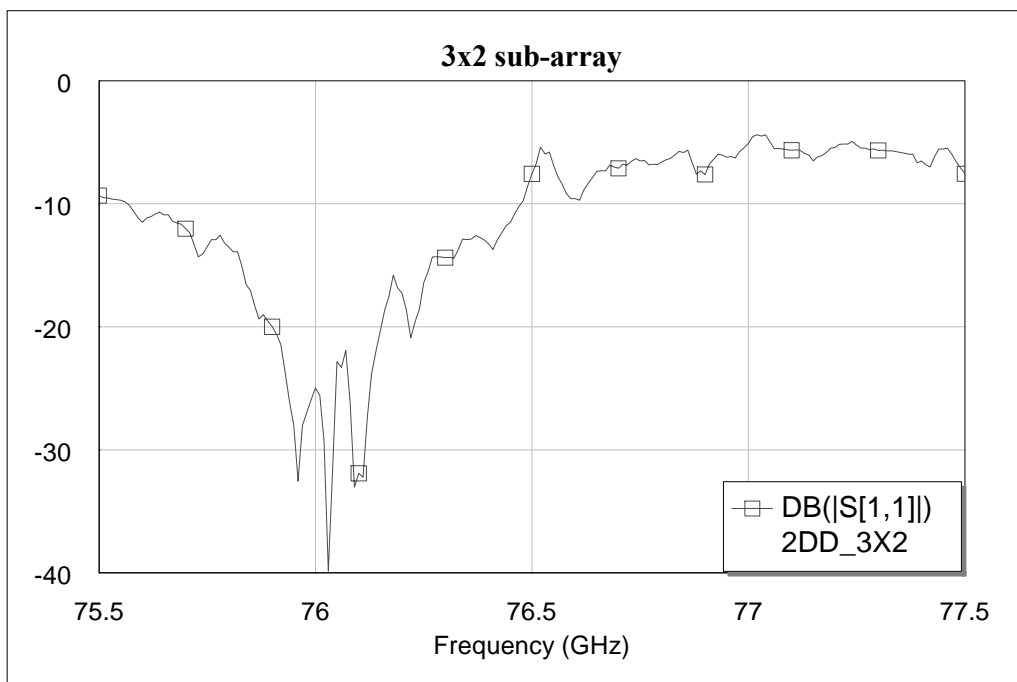

Fig. 4-6: 3x2 series fed array

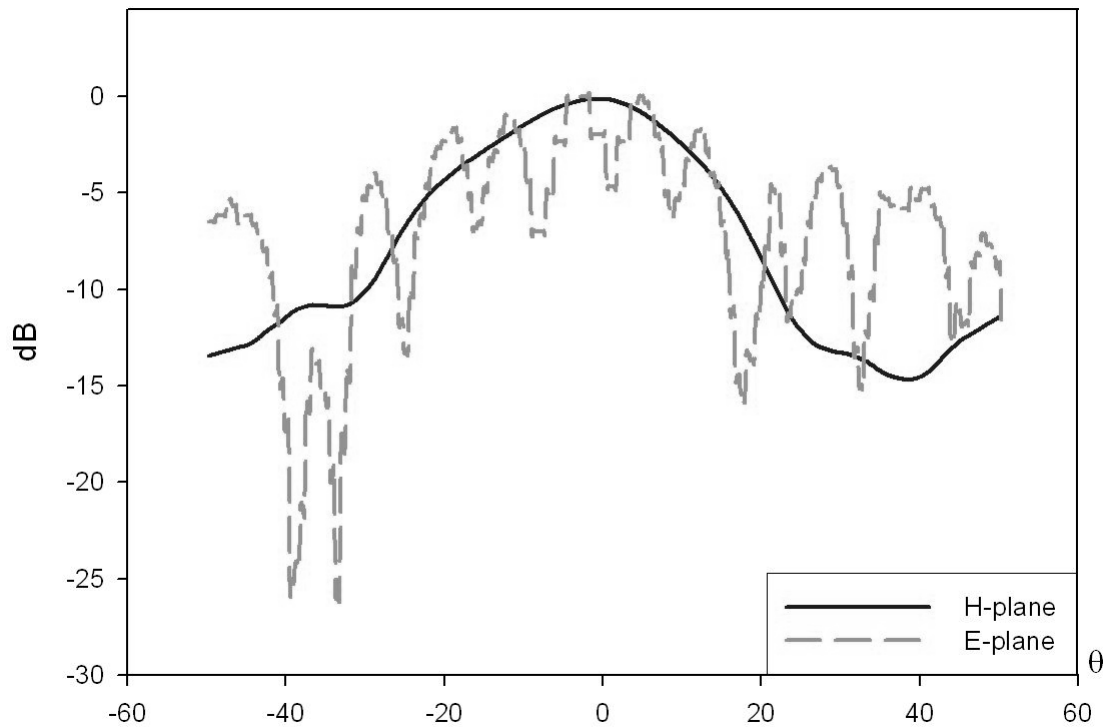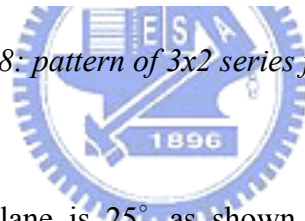*Fig. 4-7: return loss of 3x2 series fed array*

Fig. 4-8: pattern of 3x2 series fed array

The beamwidth of H-plane is 25° as shown in figure 4-8, and the gain is approximately 8.5 dBi. The E-plane pattern is irregular because of the scattering by the connector. Figure 4-9 and table 4-1 depict the photo of Rotman lens type 1 with antenna arrays, and the measurement resultant is shown in figure 4-10.
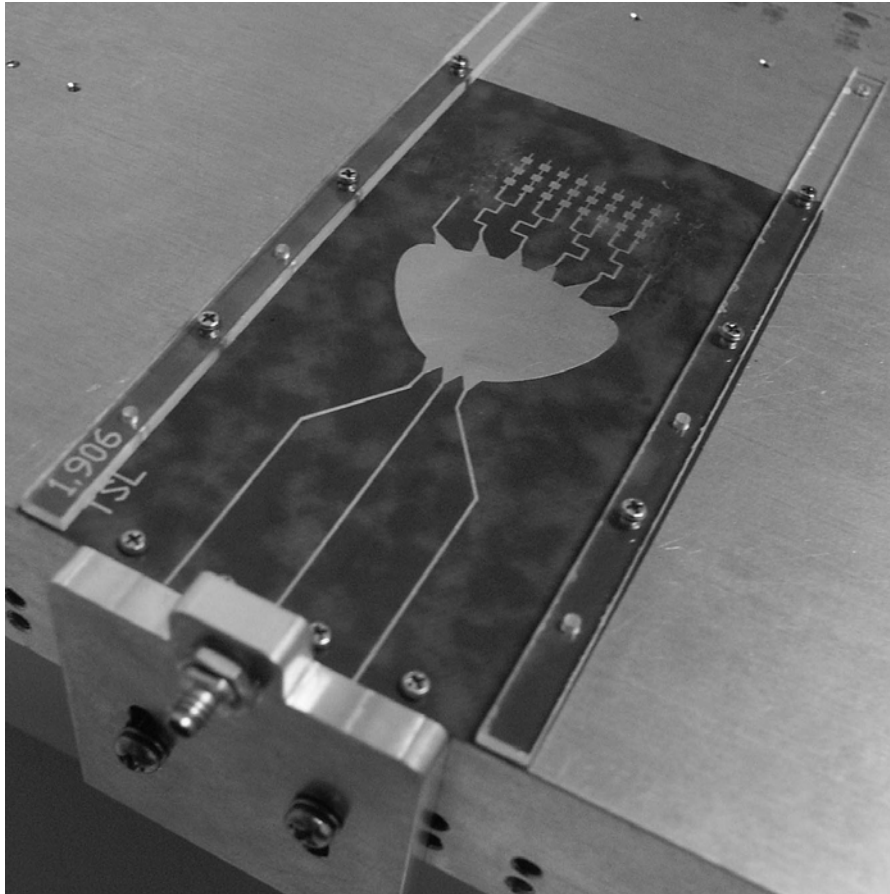
Fig. 4-9: photo of modified Rotman lens type 1

4 5 6 7 *(lens shape)* 2 1 3	Port 1	Port 2	Port 3	Port 4	Port 5	Port 6	Port 7
X	0.00	0.28	0.28	19.18	19.90	19.90	19.18
Y	0.00	2.35	-2.35	5.70	2.00	-2.00	-5.70

(Dimensions in mm)

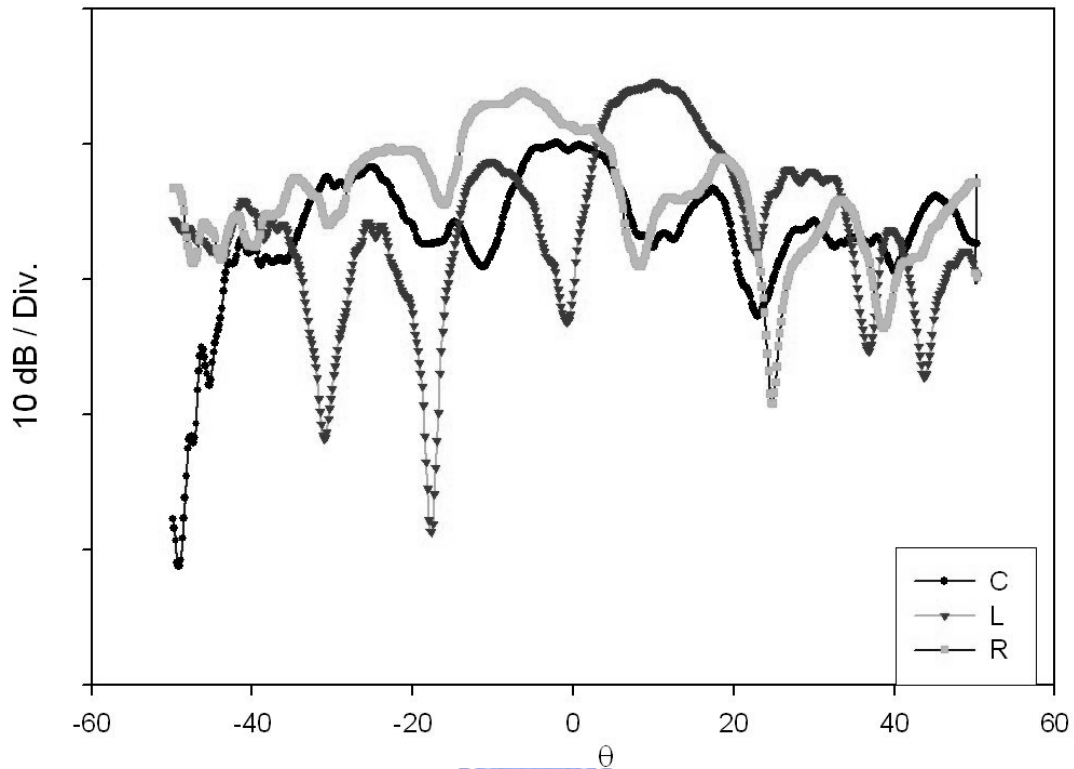*Table 4-1: configuration of modified Rotman lens type 1*

Fig. 4-10: normalized pattern of the Rotman lens type 1 with 4 sub-arrays

The Rotman lens fed array type 1 is designed with $\alpha=9^\circ$, $\beta=7.5^\circ$, G=20mm, and g=1.006. Figure 4-10 clearly displays that the main beam shifted with the changing of feeding point, main beam indicates -1.86° for central port, and 10.33°, -6.27° for left port and right port respectively, note that there are about 5dB difference between the central feeding situation and both side feeding situations.

Rotman lens type 1 is simulated with HFSS and calculated the overall pattern with the 3x2 sub-array pattern, figure 4-11 shows the phase relationships and figure 4-12 displays the calculated pattern,

(a)

Plot 1 : S Matrix Data
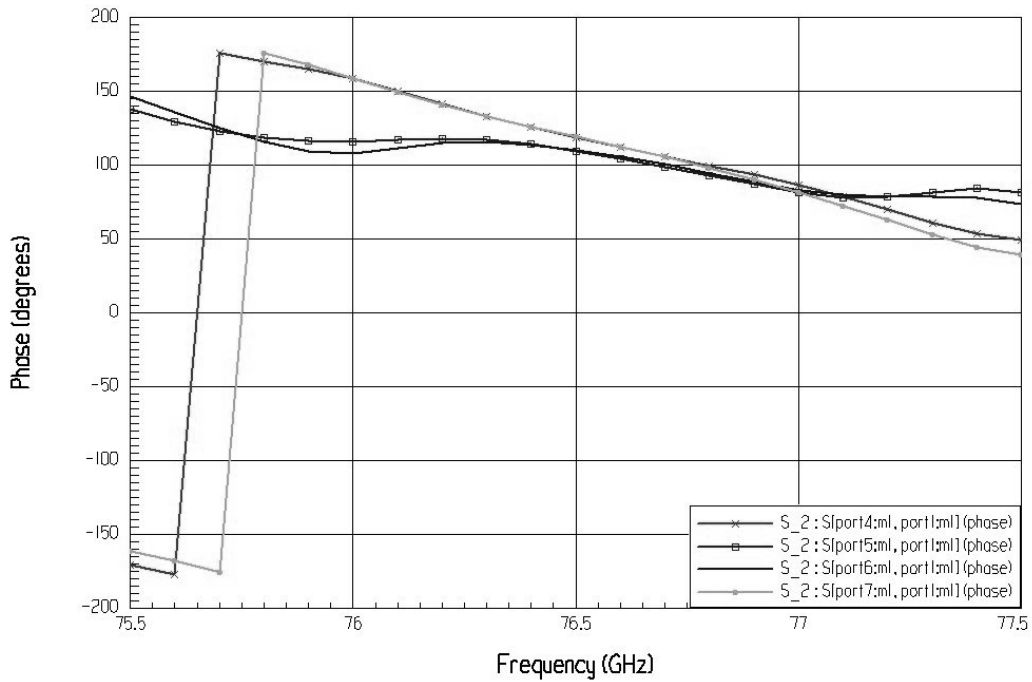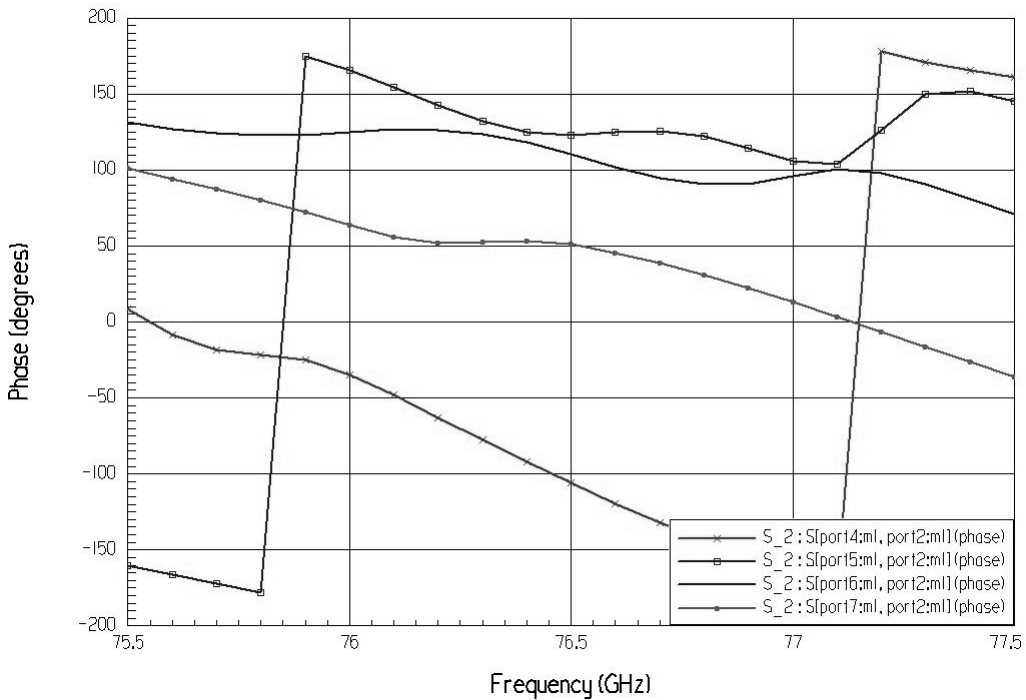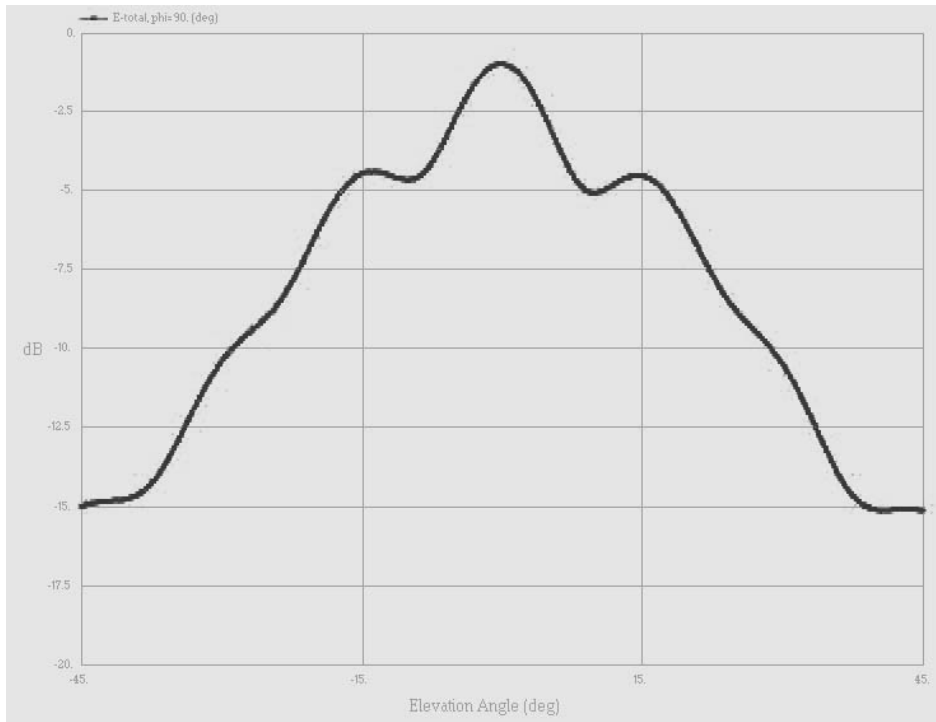

(b)

Plot 2 : S Matrix Data

Fig. 4-11: phase relationships of Rotman lens type 1: (a) central port, and (b) side port
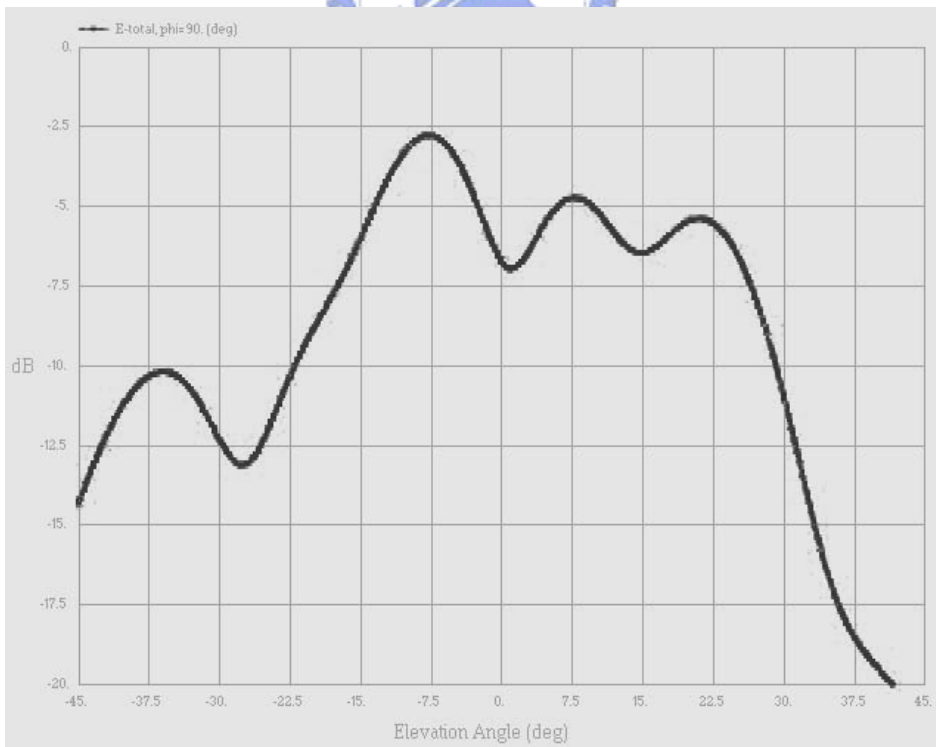
(a)

(b)

Fig. 4-12: calculated patterns: (a) central port, and (b) side port

Comparing the results, the calculated pattern manifests a highly agreement with the measured pattern, simulating results show abnormal power distribution and phase outcome, port 4 and port 7 (reference to table 4-1) obtained more power then port 5 and port 6 during central feeding; on the other hand, phase difference of port 6 and port 7 is just as designed, but disorderly for port 4, port5 and port 6, it may be as result of the side wall reflection, serious multi-path effect influences both amplitude and phase and bring these results. A simple simulation is carried out for this assumption, lens contour is expanded while the port positions are unchanged, the result is displayed in figure 4-13 and shows that phase difference of array ports excited by the side port are much closer to the designed phase difference.
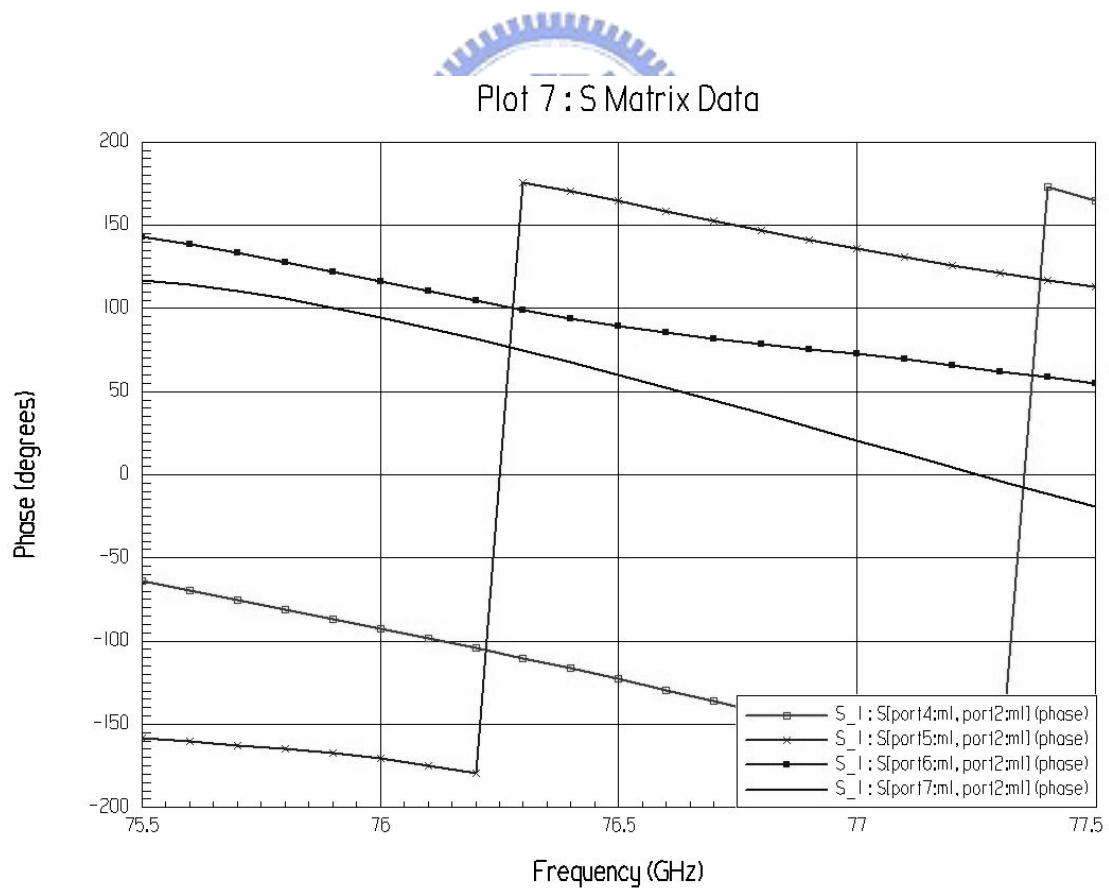

Fig. 4-13: phase relationships of expanded Rotman lens type 1 related to side port

Lens type 2 improve the drawbacks of type 1, the focal length and length/width ratio of lens are reduced, expected for lower loss and less multi-path effect. The antenna sub-array is also changed to narrow beam array composed of the tapered array mentioned in chapter 3, two tapered arrays are combined by a power divider too, and figure 4-14 shows the return loss and pattern of the array, the beam width is about 4° for E-plane, 42° for H-plane, the antenna gain is approximately 19dBi.
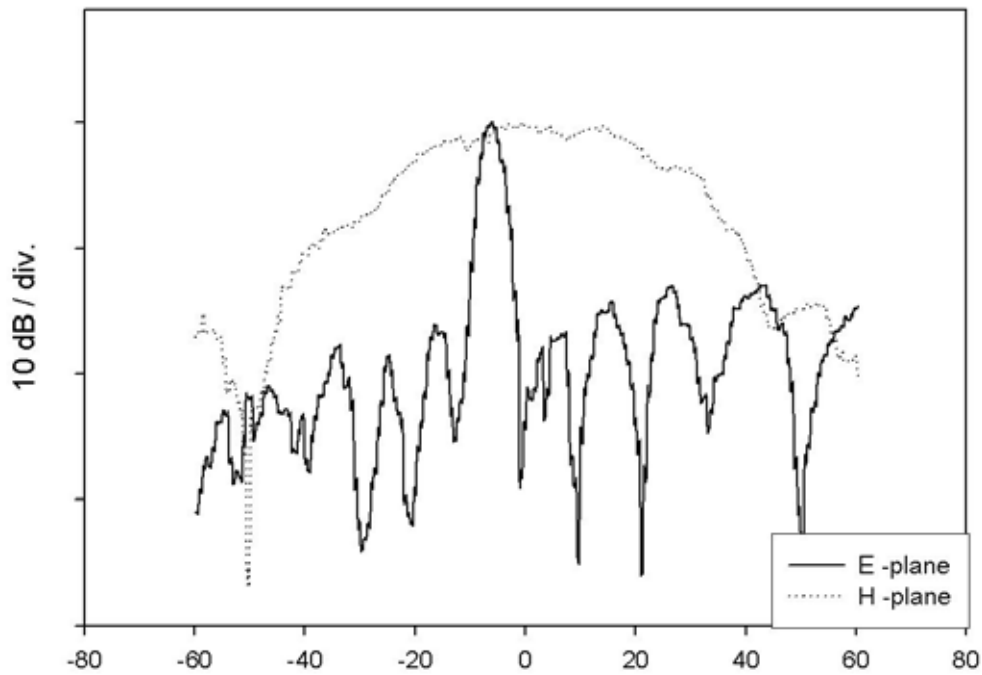
(a)
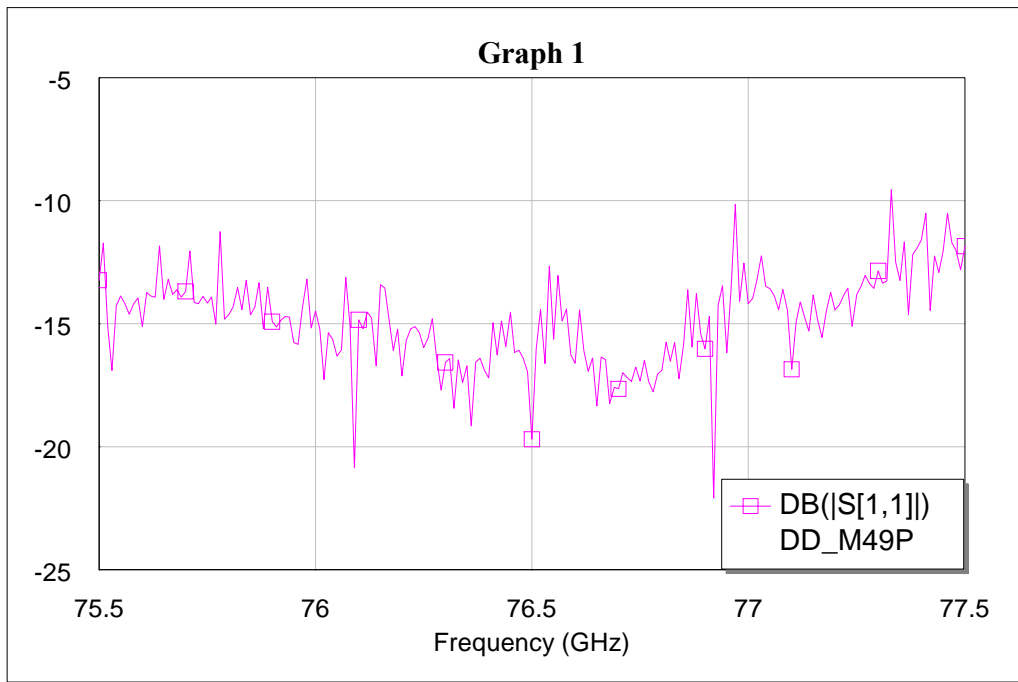
(b)

Fig. 4-14: measured of a pair of tapered array, (a) return loss and (b) pattern
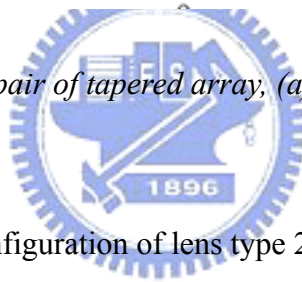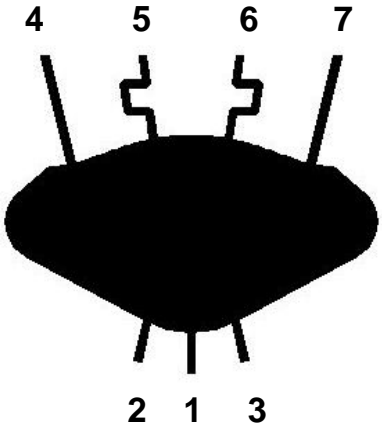
Table 4-2 depicts the configuration of lens type 2

	Port 1	Port 2	Port 3	Port 4	Port 5	Port 6	Port 7
X	-10.00	-9.46	-9.46	-1.45	-0.19	-0.19	-1.45
Y	0.00	2.26	-2.26	,6.14	1.94	-1.94	-6.14

(Dimensions in mm)

Table 4-2: configuration of lens type 2

The lens type 2 (figure 4-15) is designed with $\alpha = 18, \beta = 15°$, G=10mm, and g=1.0275. Figure 4-16 displays the pattern of this lens, fig. 4-16 (a) shows the E-plane pattern with a 4° main beam and fig. 4-16 (b) illustrates shifted patterns respected to different feeding point, main beam indicates 1.0168° for central port, and 16.10°, -7.50° for left port and right port respectively, and no more then 2dB for difference between the central feeding situation and both side feeding situations.
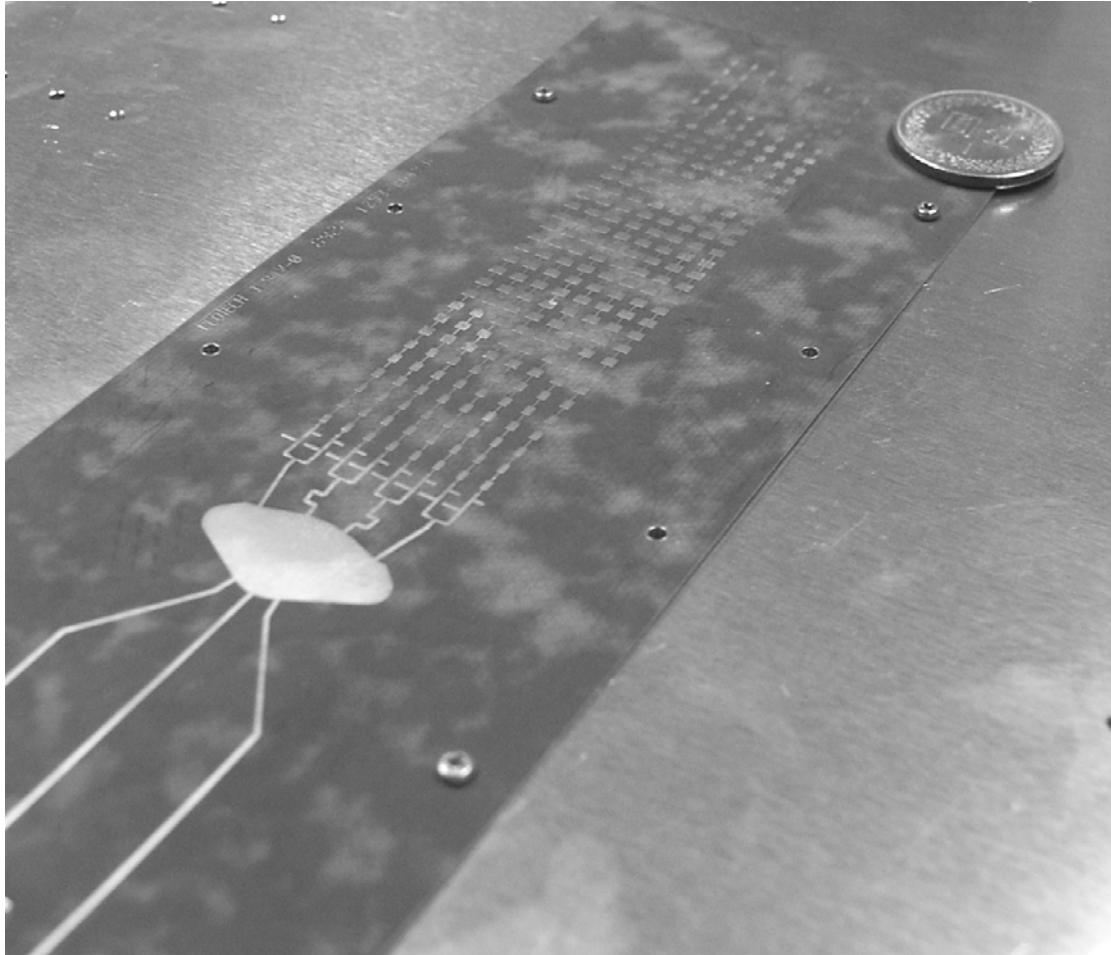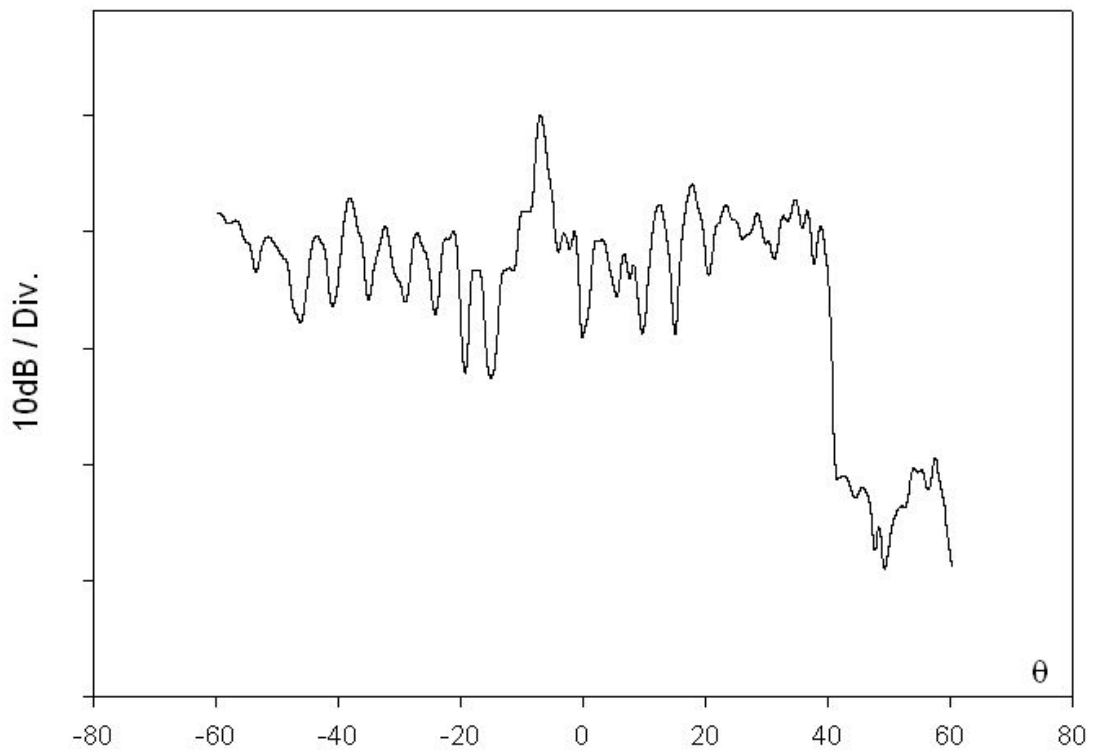

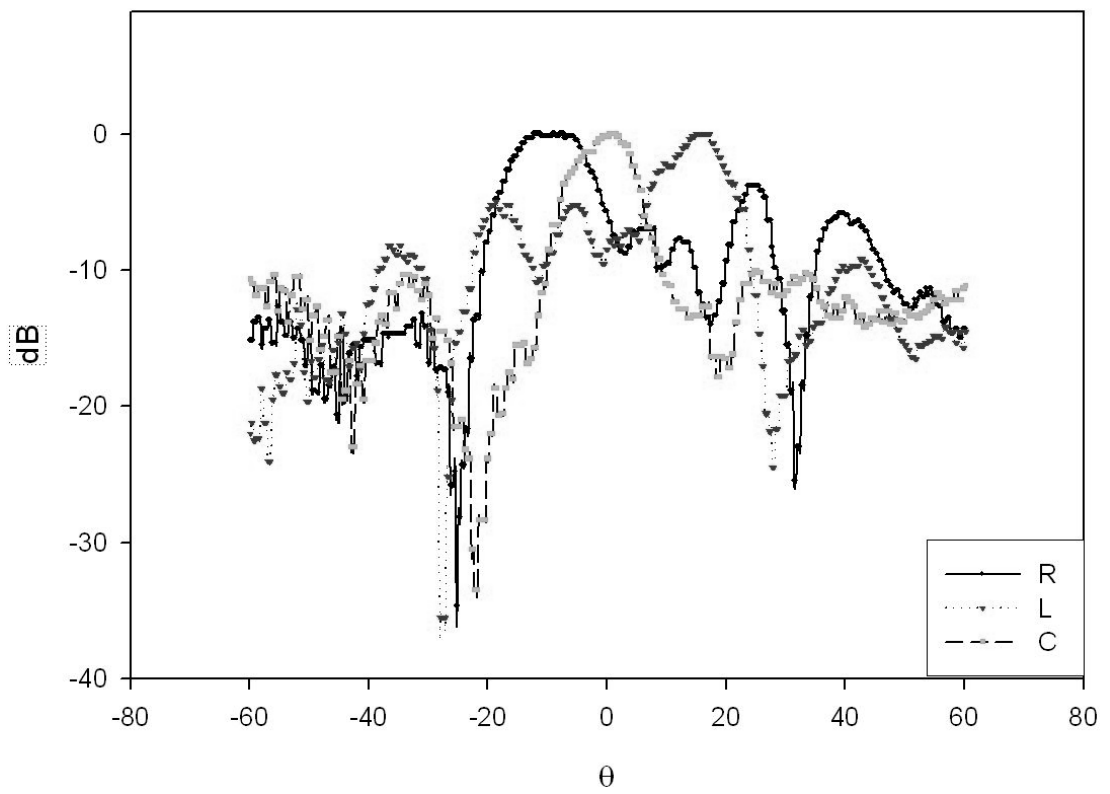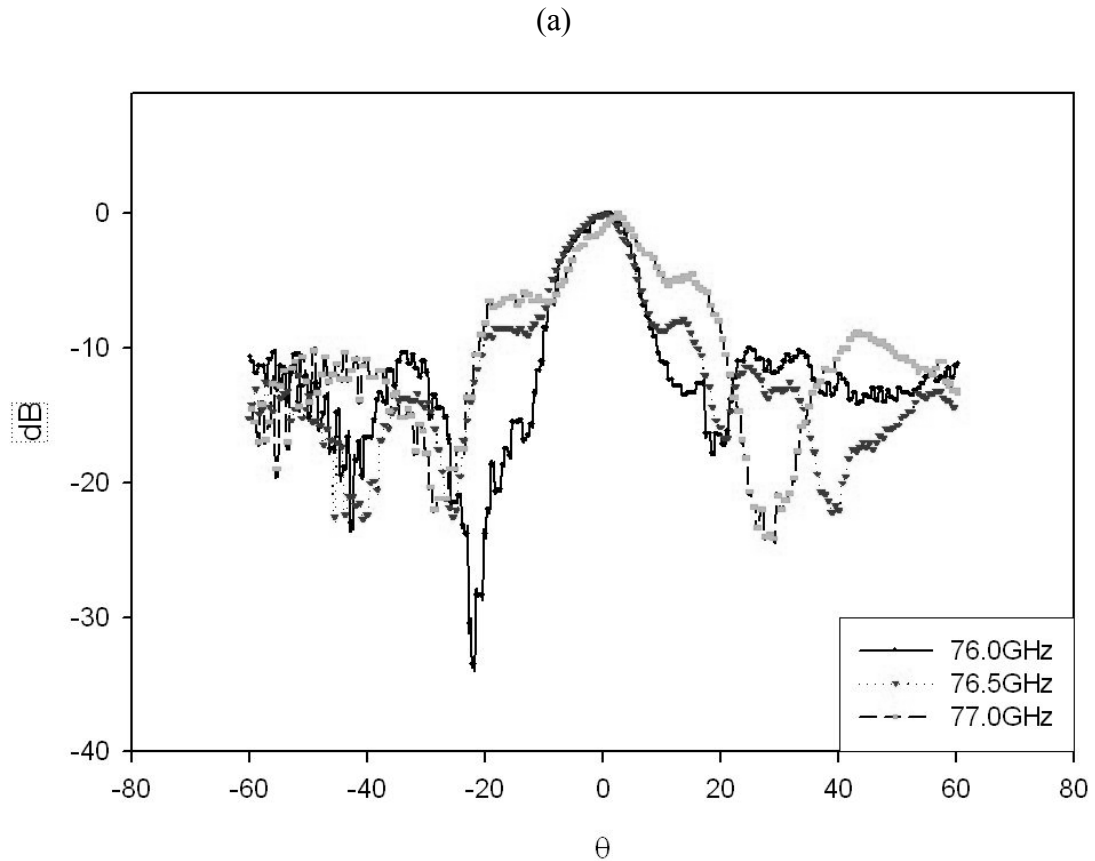*Fig. 4-15: photo of lens type 2*

(a)

(b)

Fig. 4-16: measured pattern of lens type 2 at 76GHz, (a) E-plane and (b) H-plane

The lens contour is calculated based on wave length; the frequency does affect the pattern as shown in figure 4-17, side lobe level increasing with frequency for both feeding situations.

(a)
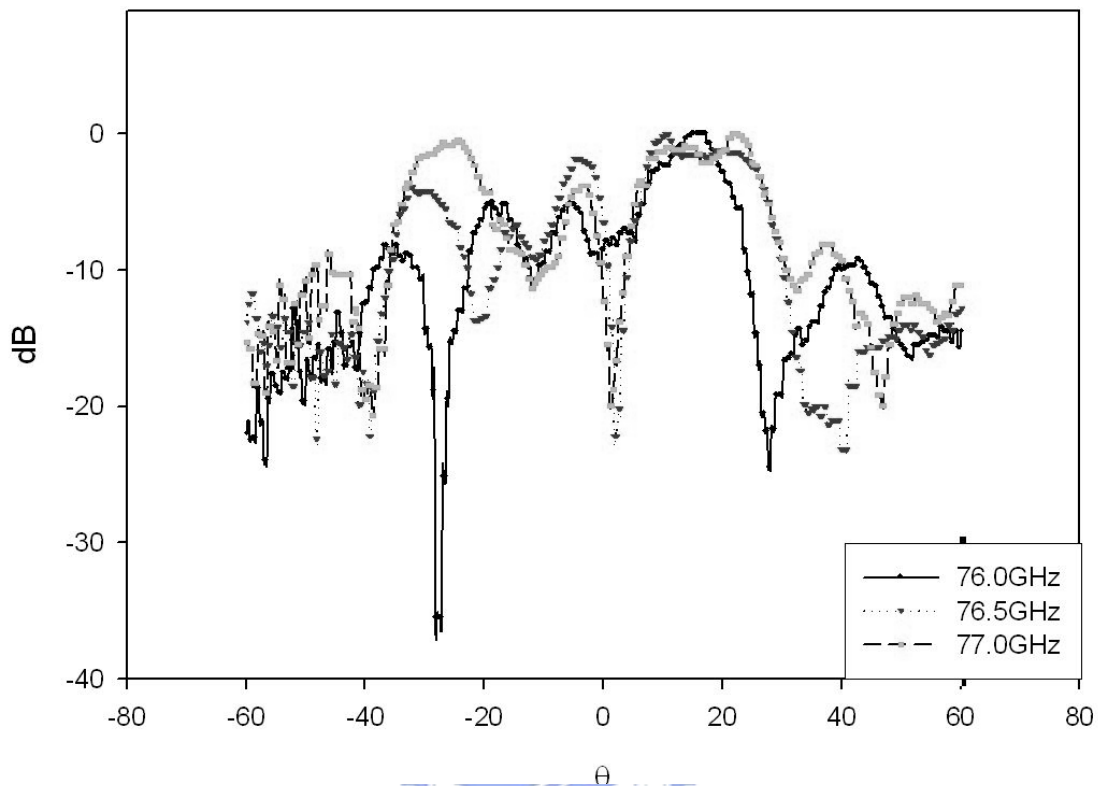
Fig. 4-17: pattern of lens type 2 vs. frequency, (a) central fed and (b) left-side fed

To obtain narrow beam, more element number is the direct option, lens type 3 contains 20 tapered pairs (means 40 tapered arrays included), and thus narrow beams for both E-plane and H-plane are expected.

Lens type 3 is a full size beam-switch array with 5 input ports to produce 5 beams pointing of different directions. The design parameter and lens contour are shown in table 4-3; the photo of the completed array is displayed as figure 4-18:

$\alpha = 12°;\quad \beta = 7.5°;\quad G = 40;\quad g = 1.01;$		
input ports		
x	y	direction of output beam
-36.35	11.55	15.2° (*non-focal port)
-39.08	6.02	7.5°
-40.00	0	0°
output ports		
x	y	w
-0.03	1.45	0.003
-0.24	4.37	0.009
-0.66	7.29	-0.0054
-1.29	10.21	-0.0361
-2.10	13.16	-0.1234
-3.08	16.16	-0.3254
-4.16	19.29	-0.7502
-5.25	22.70	-1.6161
-6.12	26.78	-3.4232
-6.10	32.65	-7.5876

(Dimensions in mm)

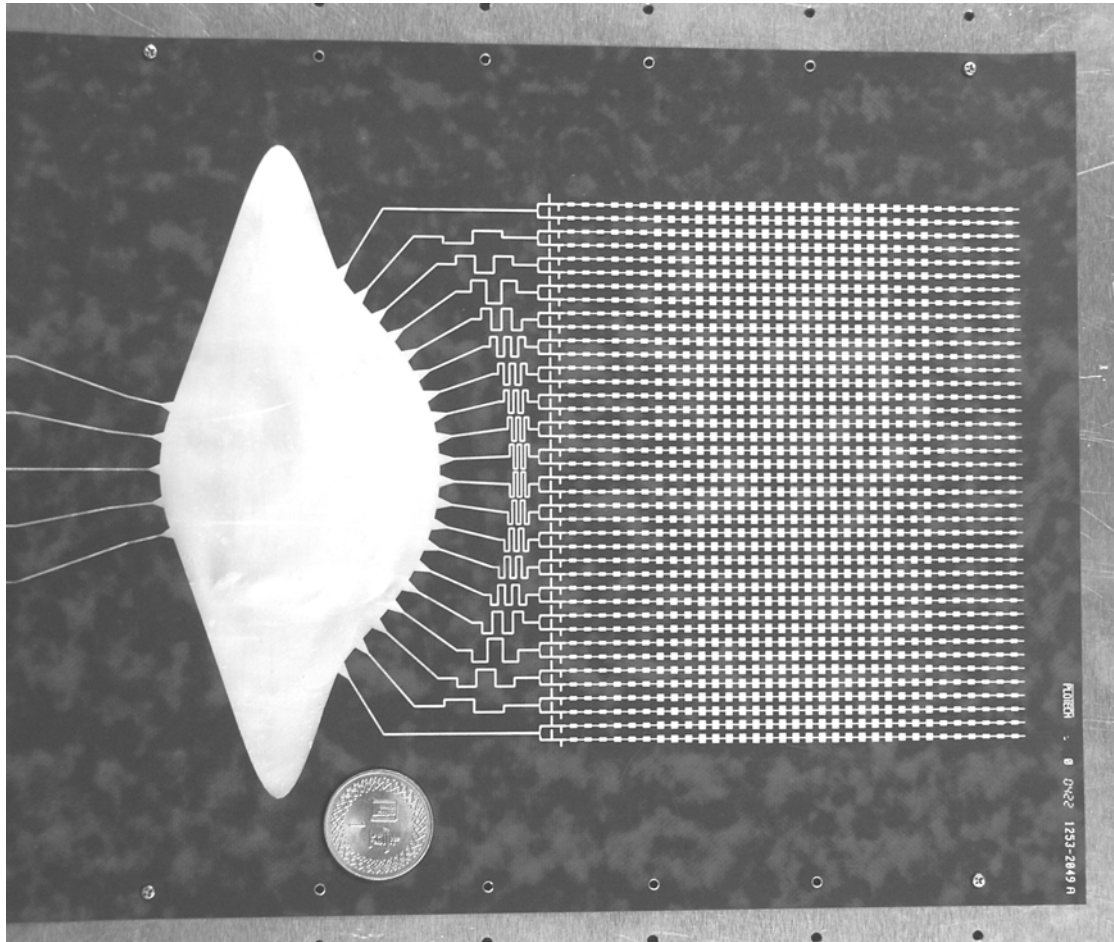*Table 4-2: configuration of lens type 3*

Fig. 4-18: photo of lens type 3

Due to the fundamental of the Rotman lens equations, only feeding from the focal points result in none phase error for all array ports, phase error is inevitable for feeding from non-focal port, figure 4-19 illustrates the calculated phase error at array ports fed by the non-focal input port.
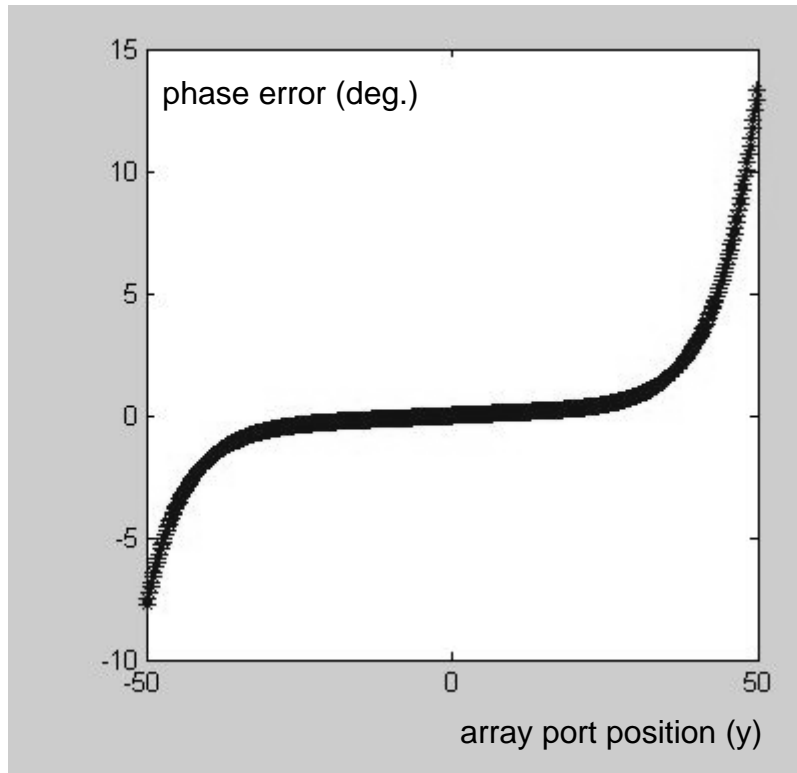
Fig. 4-19: phase error due to non-focal input port

Tuning the focal length ratio (g) does obviously improve phase error, but changes the lens contour at the same time. A well lens design requires less phase error and flat array ports at the same time, contour in figure 4-18 is a compromise for these requirements. (Note that a contour of flat array ports shortens the meander lines, in other words, reduces the loss.)

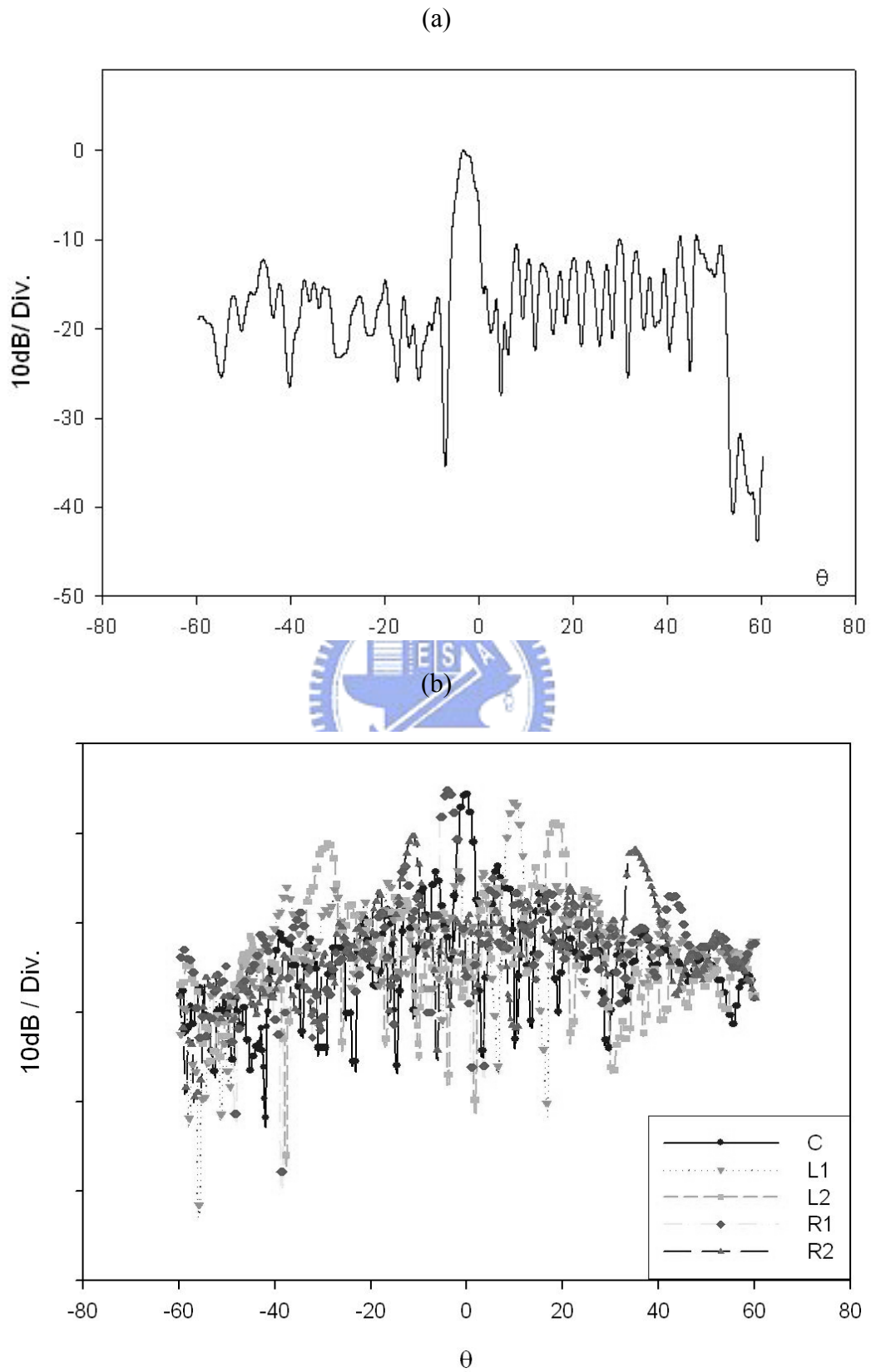Figure 4-20 depicts the measurement of lens type 3 at 76GHz:

(a)

(b)

Fig. 4-20: measurement of lens type 3, (a) E-plane, (b) H-plane

The measurements tells that the main beam for this array is 4° in E-plane, the main beam indicates -0.2° for central port (beamwidth=2.34°), 9.7° (beamwidth=2.88°) and -3.9° (beamwidth=3.02°) for first side ports, 18.7° (beamwidth=2.71°) and -11.2° (beamwidth=2.71°) for second side ports. It is interesting that a huge side lobe appears for both non-focal ports, and compare with figure 4-21 measured at 77GHz, the side lobes disappear.
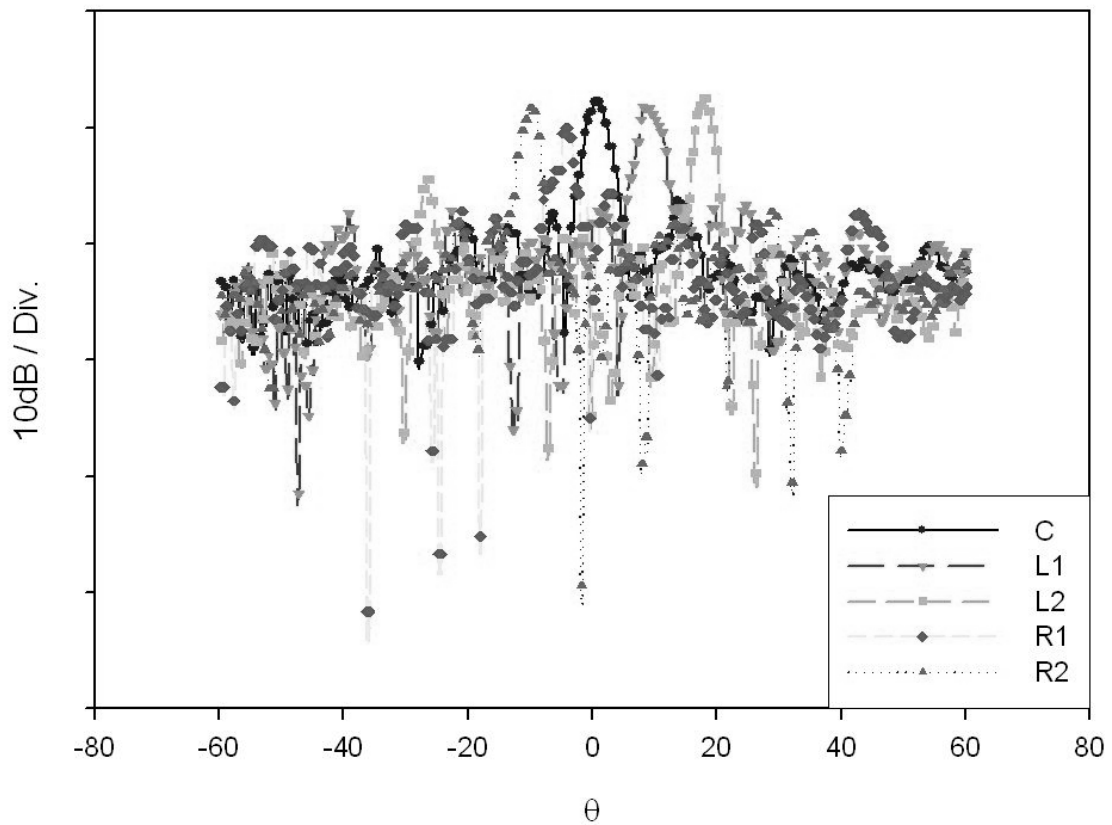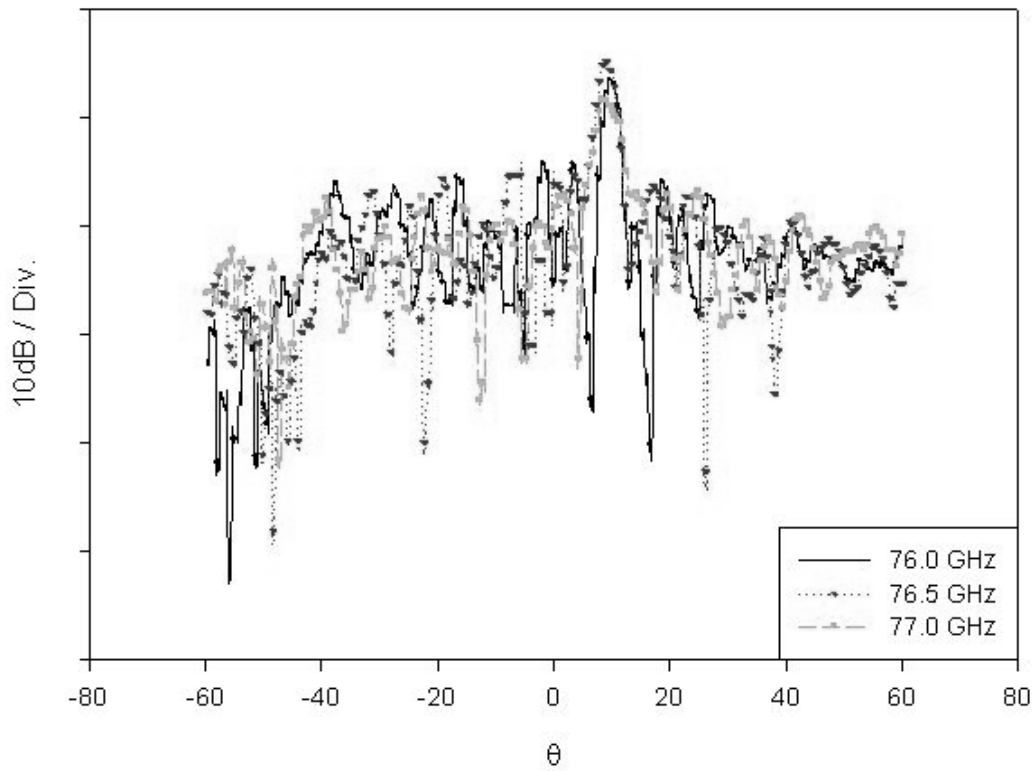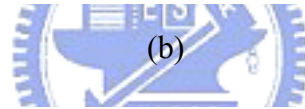

Fig. 4-21: H-plane of lens type 3 at 77GHz

To observe the diversity due to frequency, patterns of lens type 3 excited by each different port at several frequencies is shown is figure 4-22.

(a)

(b)
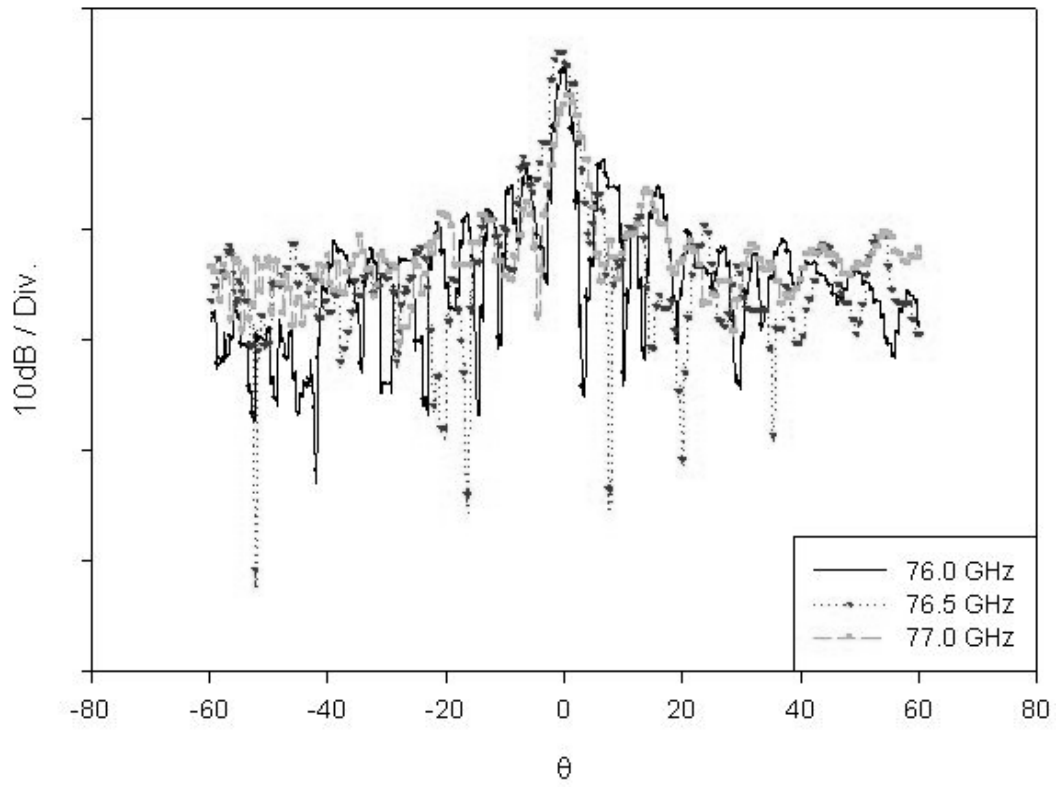
(c)

Fig. 4-22: pattern of lens type 3 vs. frequency, (a) central port, (b) 1st lift-side port and (c) 2nd lift-side port

Figure 4-22 shows clearly that the maximum main beam occurs when the side lobe is minimum, for all focal ports, better measurement happens at 76.5 GHz, and for non-focal ports, operating at 77 GHz has a better result.

Chapter 5. Conclusion

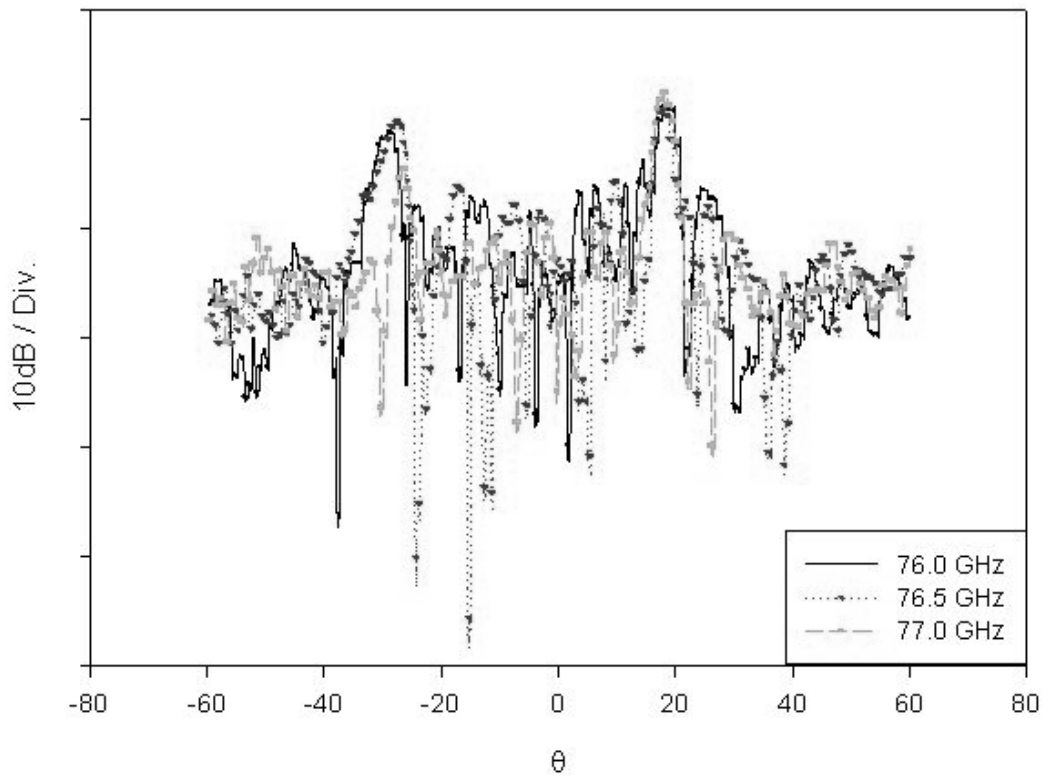A new beam-switching antenna array operating at 76-77GHz for forward-looking collision avoidance system is proposed in this thesis, the antenna array contains a modified Rotman lens as beam-switching network and tens of sub-arrays, this antenna array provides 5 switch-able directions on H-plane and forms narrow main beam for both E-plane and H-plane simultaneously.

For narrow beam applications, to construct the beam-switching network with Rotman lens is the better then using phase shifters, because plenty antenna elements are needed to form a narrow beam, and it's difficult and also expensive to build beam-switching network with phase shifters. on the other hand, it's easily to obtain more beams by simply set more input port with appropriate phase error consideration. Nevertheless, there are draw backs for Rotman lens. loss is the major issue, which could be improved with different feeding methodology; size is another problem, reducing the size may reduce the loss but raises the multi-path effect, more research on field and design of side wall could be helpful for lessening both loss and size.

Reference

1. Hermann Rohling and Ernst Lissel, "77GHz Radar Sensor for Car Application", IEEE international radar conference, 1995

2. Warren L. Stutzman, Gary A. Thiele, "Antenna Theory and Design" 2nd, John Wiley & sons, INC, 1998

3. Keith R. Carver, "Microstrip Antenna Technology", IEEE trans. Antennas Progagat., vol. AP-29 Jan. 1981

4. Anders G. Derneryd, "Linearly Polarized Microstrip Antennas", IEEE transactions on antennas and propagation, Nov. 1976

5. J. Freese, R. Fakoby, "Synthesis of Microstrip Series-fed Patch Arrays for 77GHz-sensor Applications", microwave conference, 2000

6. W. Rotman and R. F. Turner, "Wide-Angle Microwave Lens for Line Source Applications", IEEE Trans. Antennas Propagat., vol. AP-11, pp.623-632, Nov. 1963

7. R.C. Hansen, "Design Trades for Rotman Lenses", IEEE Trans. Antennas Propagat., vol. 39, NO. 4, Apr. 1991

8. *Rohling, H.; Lissel, E.;* "77 GHz radar sensor for car application," Radar Conference, 1995

9. Wolfgang Menzel, Dietmar Pilz, and Ralf Leberer, "A 77 GHz FMCW radar front-end with a low-profile low-loss printed antenna," 1999 IEEE MTT-S International, 1999